Inorg. Chem. **2008**, *47*, 8526−8542

Forum

Increasing the Structural Complexity of Chromium(IV) Oxides by High-Pressure and High-Temperature Reactions of CrO_2†

E. Castillo-Martínez, A. M. Arévalo-López, R. Ruiz-Bustos, and M. A. Alario-Franco*

Departamento de Química Inorgánica I, Universidad Complutense de Madrid, 28040 Madrid, Spain

Received June 2, 2008

This work presents an overview of a series of increasingly complex oxides synthesized from CrO_2, under high-pressure and high-temperature conditions, having Cr^{4+} in octahedral coordination. Although the emphasis is on the structure and microstructure of the compounds as obtained from X-ray diffraction and transmission electron microscopy and diffraction, attention is also given to their interesting electronic and magnetic properties. The study is complemented with an electron energy loss spectroscopic analysis of the different phases. These are the cubic perovskite $SrCrO_3$, the orthorhombic perovskite $CaCrO_3$, the solid solution $Sr_{1-x}Ca_xCrO_3$, the Ruddlesden−Popper-type $Sr_3Cr_2O_7$, the family $CrSr_2RECu_2O_8$ (RE = rare earth), a compositionally modulated perovskite "$PbCrO_3$", and the misfit layer oxide $SrO_2[CrO_2]_{1.85}$.

Introduction

Transition elements show a fascinating chemistry for many reasons, among which obviously presides the variety of oxidation states that they show, brilliantly dressed by their wide-ranging coordination environments and their assorted relative stabilities. Even with just one "ligand", oxygen, one can find many different oxides that show an uncountable number of useful properties. It is, in fact, one of the principal roles of Solid State Inorganic Chemistry to establish categories and behavioral patterns among such a fertile territory, in which the structure is one of the brighter aspects. For a non-connoisseur, it is perhaps surprising that, just in oxides, one can have up to 12 types of coordination polyhedra and up to 8 types of oxidation states. Putting aside the more specialized aspect of why these are not universal for all transition elements, i.e., each one of them has its own particular chemistry, there is still plenty of beauty in the way that these polyhedra combine in several ways and dimensions so as to set up the truly spectacular diversity of the oxide crystal structures.

The case of chromium is paradigmatic of this kind of behavior, and one can have oxides of this element, number 24, and electron configuration $[Ar]3d^54s^1$ in oxidation states ranging from II to VI and coordination polyhedra that are essentially octahedra and tetrahedra. If the oxides are binary, the number of compounds is rather limited,[1] being essentially Cr_2O_3 ($^{VI}Cr_2^{3+}O_3$), Cr_2O_5 ($^{VI}Cr_2^{3+}\ ^{IV}Cr_4^{6+}O_{15}$), Cr_3O_8 ($^{VI}Cr_2^{3+}\ ^{IV}Cr_7^{6+}O_{24}$),[2] later on determined to be Cr_8O_{21},[3] Cr_5O_{12} ($^{VI}Cr_2^{3+}\ ^{IV}Cr_3^{6+}O_{12}$),[4] CrO_2 ($^{VI}Cr^{4+}O_2$), and CrO_3 ($^{IV}Cr^{6+}O_3$),[5] where the roman superscript at the left of Cr implies the coordination polyhedra in the particular oxidation state as indicated by the right-side arabic numeral.

In a somewhat restrictive sense, there are then only three binary chromium oxides: Cr_2O_3, CrO_2, and CrO_3. However, on a more general basis and taking as binary the "mixed" chromium(III)/chromium(VI) oxides, the total number of *simple* chromium oxides is double: six in all. Although neither $Cr^{2+}O$ nor $Cr_2^{5+}O_5$ forms, there are a restricted

† Dedicated to Prof. J. B. Goodenough and Prof. B. L. Chamberland.

* To whom correspondence should be addressed. E-mail: maaf@quim.ucm.es.

(1) Kubota, B. *J. Phys. Soc. Jpn.* **1960**, *15*, 1706.
(2) Hewston, T. A.; Chamberland, B. L. *J. Magn. Magn. Mater.* **1984**, *43*, 89–95.
(3) Norby, P.; Nørlund Christensen, A.; Fjellvåg, H.; Nielsen, M. *J. Solid State Chem.* **1991**, *94*, 281–293.
(4) Wilhelmi, K. A. *Acta Chem. Scand.* **1965**, *19*, 165–176.
(5) Stephens, J. S.; Cruickshank, D. W. J. *Acta Crystallogr., Sect. B* **1970**, *26*, 222–226.

10.1021/ic801015b CCC: $40.75
Published on Web 09/29/2008

number of ternary chromium(II) oxides,[6] and a few more of chromium(V) exist.[7] It is certainly worth noting that chromium is the only 3d transition metal that does not seem to form a monoxide.[8] On the contrary, the ternary oxides of chromium(III), -(IV), and -(VI) are rather numerous, and their abundance follows approximately that order.

To categorize the relative stability of these oxidation states, one often relies on the Frost diagrams (see, e.g., ref 9), notwithstanding the fact that these are established from the redox equilibria in solution. The Frost diagram for chromium indicates that the most stable oxidation state is indeed Cr^{III} and that the highest one, Cr^{VI}, is very oxidizing. However, it also shows that both Cr^{IV} and Cr^{V} are unstable with respect to disproportionation in Cr^{III} and Cr^{VI}, something that is well substantiated in the formulas of the intermediate oxides indicated above and in the fact that, in order to obtain pure CrO_2, high pressure is needed.[10]

CrO_2 was first synthesized in 1859 by Wöhler,[11] and in view of its interesting—and rather exceptional—properties, much work has been dedicated to it.[12] It has the rutile-type crystal structure,[13] and as a significant fundamental material, it is a distinguished member of the restrictive club of half-metallic ferromagnets at room temperature.[14] This effect, a 100% spin polarization of conduction electrons, enhances the giant magnetoresistance and has made a revolution into the storage capabilities on the actual hard disk drives and magnetic sensors.[15] As a consequence of its magnetic properties, CrO_2 is used in magnetic recording and storage and, in spite of the large-scale synthesis difficulties, it is made in industrial amounts.

As one would expect, the chemistry of Cr^{IV} becomes richer and structurally more complex when CrO_2 is reacted with other chemicals so as to make mixed oxides. We have been working for some time on the synthesis of perovskite-related materials by reacting at high pressure and high temperature mixtures of CrO_2 with different oxides. It is well-known that the study of transition-metal oxides with perovskite and related structures has attracted much attention in recent years because of the wide range of interesting properties observed in these apparently "simple" structures.[16,17]

Concerning the simplest $M^{II}Cr^{IV}O_3$ perovskites, those with M = Sr, Ca, and Pb were first synthesized under high pressure and high temperature in the late 1960s.[18−20] Then, a kind of a temporal parentheses took place in their study. However, there has recently been a renewed interest on the two alkali-earth chromates(IV)[21−25] in view of their interesting electronic properties. Our interest in these materials also comes from trying to expand the corresponding phase diagrams in the search for new phases. We have, indeed, found new misfit-layer-type structures as well as some novel phases of the Ruddlesden−Popper (RP) type in the $Sr-Cr^{IV}-O$ system.[26,27]

In the case of the lead perovskites (which include the celebrated highly distorted and ferroelectric $PbTiO_3$), the less well-known $PbCrO_3$ has repeatedly been claimed to be cubic (space group $Pm\bar{3}m$), although a large broadening of the diffraction peaks had been noticed.[8,20,28] However, in none of these studies, neither was the precise stoichiometry established nor was a microstructural analysis performed. As we have recently reported, its real stoichiometry and structure are far more elaborated than those of a simple cubic perovskite.[29]

A somewhat more common, yet very interesting, structural complexity is also observed when CrO_2 reacts with more than one single oxide. This is clearly observed in the family of chromo(IV) cuprates: $CrSr_2RECu_2O_8$ (Cr-1212, RE = rare earth), of which we have recently prepared 11 members.[30] Although nonsuperconducting, these are interesting examples of the very large family of cuprates that have so often been studied in the last few years. In this particular case, the so-called charge-reservoir layer[31] contains $[Cr-O_6]$ octahedra. This gives a stoichiometry $MSr_2RECu_2O_8$ closer to perovskite than the usual cuprates, e.g., $YBaCu_2O_7$. Also, they constitute a triple superstructure of the perovskite due to the ordering found in both the A and B positions and the oxygen sublattice.

We describe and discuss in this paper all of these chromium(IV) compounds, from the *simple* basic perovskites $ACrO_3$ (A^{II} = Ca, Sr, and Pb) to the more elaborated misfit-layer compound $[Sr_2O_2][CrO_2]_{1.85}$, through a number of other

(6) Saes, M.; Raju, N. P.; Greedan, J. E. *J. Solid State Chem.* **1998**, *140*, 7–13.
(7) Saez-Puche, R.; Jimenez, E.; Isasi, J.; Fernandez-Díaz, M. T.; García-Muñoz, J. L. *J. Solid State Chem.* **2002**, *171*, 161.
(8) Goodenough, J. B.; Kafalas, J. A.; Longo, J. M. In *Preparative Methods in Solid State Chemistry*; Hagenmuller, P., Ed.; Academic Press: London, 1972.
(9) Shriver, D. F.; Atkins, P. W. *Inorganic Chemistry*, 3rd ed.; OUP: Oxford, U.K.; 1999; p 294.
(10) Chamberland, B. L. *Crit. Rev. Solid State Mater. Sci.* **1977**, *1*, 1–31.
(11) Wohler, F. *Ann. Chem.* **1859**, *111*, 117.
(12) Michel, A.; Benard, J. *C. R. Acad. Sci. Paris II* **1935**, *200*, 1316.
(13) Porta, P.; Marezio, M.; Remeika, J. P.; Dernier, P. D. *Mater. Res. Bull.* **1972**, *7*, 157.
(14) De Groot, R. A.; Mueller, F. M.; Engen, P. G.; Buschow, K. H. *Phys. Rev. Lett.* **1983**, *50*, 2024–2027.
(15) Hwang, H. Y.; Cheong, S. W. *Science* **1997**, *278*, 1607–1609.
(16) Goodenough, J. B. *Rep. Prog. Phys.* **2004**, *67*, 1915–1993.
(17) Mitchell, R. H. *Perovskites. Modern and Ancient*; Almaz Press Inc.: Ontario, Canada, 2002.
(18) Chamberland, B. L. *Solid State Commun.* **1967**, *5*, 663–666.
(19) Kafalas, J. A.; Goodenough, J. B.; Longo, J. M. *Mater. Res. Bull.* **1968**, *3*, 471.
(20) Roth, W. L.; DeVries, R. C. *J. Appl. Phys.* **1967**, *38*, 951.
(21) Williams, A. J.; Gillies, A.; Attfield, J. P.; Heymann, G.; Huppertz, H.; Martinez-Lope, M. J.; Alonso, J. *Phys. Rev. B* **2006**, *73*, 104409.
(22) Zhou, J. S.; Jin, C. Q.; Long, Y. W.; Yang, L.-X.; Goodenough, J. B. *Phys. Rev. Lett.* **2006**, *96*, 046408.
(23) Ortega-San-Martin, L.; Williams, A. J.; Rodgers, J.; Attfield, J. P.; Heymann, G.; Huppertz, H. *Phys. Rev. Lett.* **2007**, *99*, 255701.
(24) Castillo-Martinez, E.; Durán, A.; Alario-Franco, M. A. *J. Solid State Chem.* **2008**, *181*, 895–904.
(25) Komarek, A. C. et al. arXiv:0804.1071v1 [cond-mat.str-el].
(26) Castillo-Martínez, E.; Alario-Franco, M. A. *Solid State Sci.* **2007**, *9*, 564–573.
(27) Castillo-Martínez, E.; Schönleber, A.; van Smaalen, S.; Arévalo-López, A. M.; Alario-Franco, M. A. *J. Solid State Chem.* **2008**, accepted. DOI: 10.1016/j.jssc.2008.03.033.
(28) Chamberland, B. L.; Moeller, C. W. *J. Solid State Chem.* **1972**, *5*, 39–41.
(29) Arévalo-López, A. M.; Alario-Franco, M. A. *J. Solid State Chem.* **2007**, *180*, 3271–3279.
(30) Ruiz-Bustos, R.; Aguirre, M. H.; Alario-Franco, M. A. *Inorg. Chem.* **2005**, *44* (9), 3063.
(31) (a) Tokura, Y.; Takagi, H.; Uchida, S. *Nature* **1989**, *337*, 345. (b) Alario-Franco, M. A. *Adv. Mater.* **1994**, *7*, 229.

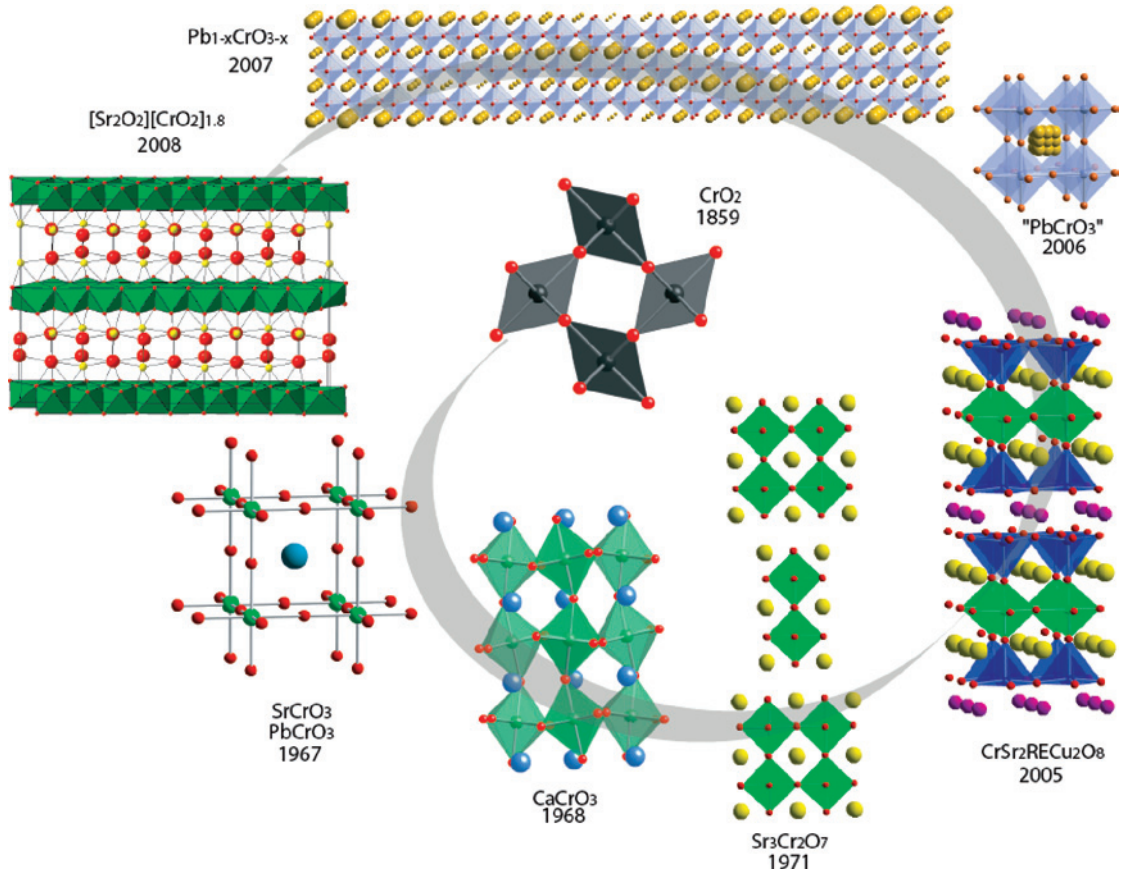

Figure 1. Structures of the different oxides studied in this paper, containing Cr^{4+} in an oxygen octahedral environment, obtained at high pressure and high temperature from CrO_2, located at the image center. The compounds are analyzed counterclockwise in order of structural complexity. This goes in parallel to the chronological order of their discovery: the year when they were first reported is also indicated, below the formula.

interesting chromium oxides such as the family Cr-1212, some RP phases, and the $(Ca-Sr)CrO_3$ solid solution that we have recently prepared.

Figure 1 shows, ordered in chronological terms and as a function of structural complexity, the crystal structures of the different mixed oxides that we have obtained working at high-pressure and high-temperature conditions using CrO_2 as a starting material. Some of these oxides were already known but not fully characterized. The majority are, however, novel and have been recently obtained in our group. They show interesting structures and properties. All of these materials have been thoroughly characterized by the usual solid-state chemistry techniques. Special emphasis has been made in the structure, microstructure, and compositional aspects of these multinary oxides using powder X-ray diffraction (PXRD) and/or single-crystal diffraction, neutron diffraction, high-resolution transmission electron microscopy (HRTEM), X-ray energy-dispersive spectroscopy (XEDS), electron energy loss spectroscopy (EELS), and selected-area electron diffraction (SAED). This has allowed us to show the rather elaborated microstructure that all but the simplest one, $SrCrO_3$ (one of the few truly cubic perovskites), do show.

We present in here a resumé of the conditions in which the syntheses of these materials have been optimized as well as some significant results that we have obtained from the point of view of their increasing structural complexity. Mention will be made to the often complex but always remarkable electronic and magnetic properties of these materials. This will be followed by a discussion of the ensemble.

This paper is dedicated to Professors J. B. Goodenough and B. L. Chamberland, who have greatly contributed to the knowledge of chromium(IV) perovskites.

Experimental Section

Samples were made at high pressures and high temperatures in a "belt"-type apparatus located in the Laboratorio Complutense de Altas Presiones (http://www.ucm.es/info/labcoap/index.htm). Details can be found in the corresponding references.

PXRD profiles were collected in Siemens D-500 and D-5000 diffractometers with the Bragg−Bentano geometry using Cu $K\alpha_1$ = 1.540 56 Å and Cu $K\alpha_2$ = 1.544 39 Å radiation and in a Phillips X'Pert PRO ALPHA 1, equipped with a Ge 111 monochromator and a fast detector X'Celerator (λ = 1.5406 Å Cu $K\alpha_1$ radiation). Data were collected in the range $5 < 2\theta < 100°$, with a step size of 0.0167° collected for 100 s.

For TEM studies, the samples were ground under liquid nitrogen and dispersed in *n*-butanol with ultrasounds. A drop of this suspension was evaporated on a cooper grid coated with holey carbon. SAED was performed in a JEOL 2000FX electron microscope, having a double tilt ±45° holder coupled with simultaneous XEDS for composition analysis. HRTEM was carried out in a JEOL 3000FEG electron microscope, with a point resolution of 1.7 Å and C_s = 0.6 mm also equipped with a XEDS detector, a double tilt ±25° holder, and an Enfina EELS system for the

Table 1. Experimental Synthesis Conditions Employed for Each of the Chromium(IV) Oxides Studied in the Present Work[a]

compound	P (kbar)	T (K)	t (min)	impurities
$SrCrO_3$	40−80	1073−1573	10	$SrO(SrCO_3) + Cr_2O_3$
$Sr_{0.8}Ca_{0.2}CrO_3$	40	1273	10	β-$CaCr_2O_4$
$Sr_{0.6}Ca_{0.4}CrO_3$	40−80	1223	10−30	β-$CaCr_2O_4$
$Sr_{0.5}Ca_{0.5}CrO_3$	50−80	1173	30	β-$CaCr_2O_4$
$Sr_{0.4}Ca_{0.6}CrO_3$	65	1173	10	β-$CaCr_2O_4$+ Cr_2O_3
$Sr_{0.2}Ca_{0.8}CrO_3$	65	1223−1273	30	β-$CaCr_2O_4$
$CaCrO_3$	80	823	15	β-$CaCr_2O_4$
$PbCrO_3$	80	1073	30	$PbO + Cr_2O_3 + Pb_5CrO_8$
$CrSr_2RECu_2O_8$	60−80	1573	30	$SrCrO_3 + CuRE_2O_4$
Sr_2CrO_4	60−65	1323	60	$Sr_3Cr_2O_8 + SrCrO_3 + SrCO_3$
$Sr_3Cr_2O_7$	65−80	1323	10	$SrCrO_3 + Sr_4Cr_3O_{10}$
$[Sr_2O_2][CrO_2]_{1.85}$	40−70	1173−1573	60−210	$SrCr_2O_4$

[a] The different columns show the following, from left to right: formula, pressure, temperature, reaction time, and impurities found in each case.

acquisition of the EELS spectra operating in the diffraction mode with a collection semiangle of 8.9 mrad.

Results

Synthesis. The first point that is worthy of comparison in these group of Cr^{IV}-based compounds is the experimental requirements and synthesis conditions.

In high pressure/high temperature synthesis experiments, it is often difficult to get pure samples, especially when one is dealing with multinary oxides. However, one can often find the best conditions so as to minimize, and eventually eliminate, impurities. Table 1 gives a synopsis of the optimum conditions to achieve the best possible samples and indicates the impurities present.

Interestingly, the preparation of the Cr-1212 phases required the cell filling to be performed in air, so as to obtain the correct stoichiometry, $CrSr_2RECu_2O_8$, while strictly the reactant composition will only give an oxygen content of 7.5 atoms/formula ($CrO_2 + 2SrO + {}^1/_2RE_2O_3 + 2CuO \rightarrow CrSr_2RECu_2O_{7.5}$).[30] The air enclosed in the cell seems to provide the necessary oxygen for the net completion because in the absence of air (cell fillings in an argon-filled glovebox) the experiments resulted in $RECrO_3$ as the main product of the reaction (having Cr^{3+}). On the other hand, if $KClO_3$ was mixed with the reactants to provide an oxygen excess and the cell was also filled in the glovebox, $SrCrO_3$ was mainly obtained. This fact indicates the high stability of $SrCrO_3$ under high oxygen pressure, a so-called "thermodynamic sink",[32] and helps us to understand why in the preparation of the solid solution $Sr_{1-x}Ca_xCrO_3$, which also required the use of a drybox for its synthesis, $KClO_3$ could not be used as an oxidizer to avoid the formation of the ubiquitous impurity β-$CaCr_2O_4$, another sink in this system!

In the Sr−Cr−O system, it is found that the RP2 phases form at higher pressure than $SrCrO_3$ and at temperatures above 1000 °C. The cubic perovskite at lower pressures and/or temperatures and the optimum conditions for the synthesis of the misfit-layer compound $Sr_2O_2(CrO_2)_{1.85}$ consists of pressures lower than those necessary for the synthesis of the RP phases and reaction temperatures and/or times longer than those at which the $SrCrO_3$ perovskite is formed. $PbCrO_3$ always required at least 80 kbar but could not be obtained above 100 kbar.

In the early work, only the rutile and single-perovskite members of Cr^{IV} were prepared and studied. We have been able to obtain a few more complex structures, and a deeper study of them and of the previously known phases has shown that the old ones were not simple either.

In what follows, the results obtained for different materials will be presented in order of increasing structural complexity.

I. Simple Perovskites: $ACrO_3$ (A = Ca, Sr, and Pb). A and B. $SrCrO_3$ and $CaCrO_3$. Structurally, $SrCrO_3$ exhibits, like $SrTiO_3$, an undistorted cubic perovskite (space group $Pm\bar{3}m$; Figure 1). In contrast, in $CaCrO_3$ (as also happens in the perovskite mineral $CaTiO_3$[33]), a distortion of the cell to an orthorhombic structure (space group $Pbnm$) is observed. This is due to the relatively small radius of Ca^{II}, which is reflected in the low value of the Goldschmidt tolerance factor[34,35] ($t_{CaCrO_3} = 0.948$; cf. $t_{SrCrO_3} = 1.003$) that increases the covalent character of the Ca−O bond, inducing a tilting of the [Cr−O_6] octahedra. There are not many cubic $SrMO_3$ perovskites at room temperature; however, a clear analogy in the structural trend is found as calcium substitutes strontium in the corresponding titanates(IV),[36] vanadates(IV),[37] and ferrites(IV).[38]

The low-temperature behavior of $SrCrO_3$ has been a matter of discussion in the recent past. Whereas Chamberland reported a Pauli paramagnetic behavior in a small single crystal,[18] recent studies in polycrystalline samples have not shown this typical metallic behavior,[21,22,26] something that could be attributed to grain-boundary scattering. However, Zhou et al. showed that an insulator-to-metal transition takes place in their polycrystalline samples under a pressure of 4 GPa.[22] It is difficult to infer, however, whether this transition is an electronic one or if it is simply due to the grain boundary being overcome by the compression, favoring the metallic behavior. Furthermore, the susceptibility measurements of the various groups showed different behavior. Zhou et al. reported a small splitting of the zero-field-cooled (ZFC)

(32) Vander Griend, D. A.; Poeppelmeier, K. R. *Int. J. Inorg. Mater.* **2001**, *3*, 1277–1282.
(33) Kay, H. F.; Bailey, P. C. *Acta Crystallogr.* **1957**, *10*, 219.
(34) Goldschmidt, V. M. *Proceedings of the Faraday Society*; Royal Society of London: London, 1929; pp 253−283.
(35) Lufaso, M. W.; Woodward, P. M. *Acta Crystallogr., Sect. B* **2001**, *57*, 725.
(36) Qin, S.; Becerro, A. I.; Seifert, F.; Gottsmann, J.; Jiang, J. *J. Mater. Chem.* **2000**, *10*, 1609.
(37) García-Jaca, J.; Mesa, J. L.; Insausti, M.; Larrramendi, J. I. R.; Arriortua, M. I.; Rojo, T. *Mater. Res. Bull.* **1999**, *34*, 289–301.
(38) Takeda, T.; Kanno, R.; Kawamoto, Y.; Takano, M.; Kawasaki, S.; Kamiyama, T.; Izumi, F. *Solid State Sci.* **2000**, *2*, 673–687.

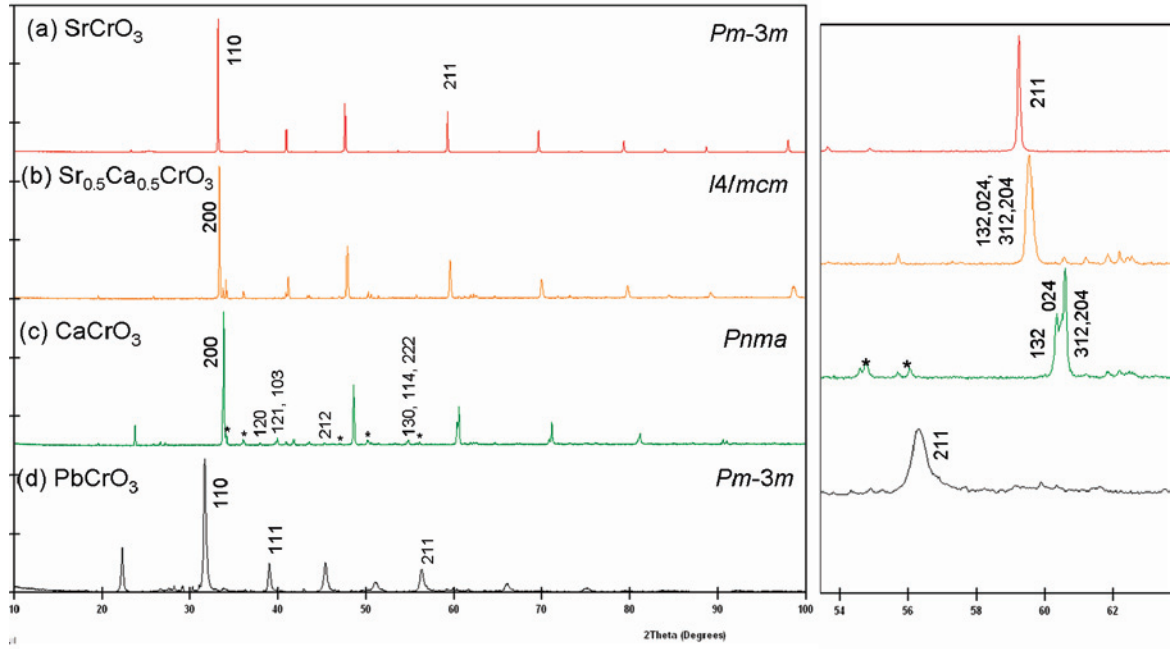

Figure 2. PXRD patterns of the "simple" perovskites: (a) $SrCrO_3$; (b) $Sr_{0.5}Ca_{0.5}CrO_3$; (c) $CaCrO_3$; (d) $PbCrO_3$. The region around the 211 reflection of the cubic perovskite is enlarged to visualize the splitting in the lower-symmetry phase, the slight broadening in the intermediate-symmetry phase, and the remarkable broadening in the modulated $Pb_{1-x}CrO_{3-x}$.

and field-cooled (FC) susceptibility curves at about 60 K,[22] which was not clearly observed in our samples.[26] Ortega-San-Martín et al.[23] recently reported that either a sharp maximum or a shoulder appears depending on the sample synthesis. This corresponds to the antiferromagnetic (AFM) ordering of the magnetic moment of one of the two unpaired electrons of the chromium in the low-temperature phase segregated with tetragonal structure, as has been previously demonstrated from neutron and synchrotron data.[23] In this last study, orbital ordering is suggested to drive a cubic to tetragonal (orbitally ordered, OO) phase transition, with the coexistence of both phases at low temperature. The phase fraction appears to depend on the pressure employed for the sample synthesis.

On the other hand, in the orthorhombic perovskite $CaCrO_3$ (space group *Pbnm*; Figure 1), first synthesized in 1968, a semiconducting behavior with AFM ordering at about 90 K was originally observed in a polycrystalline sample.[19] Later on, Weiher et al.[39] reported metallic character in, again, a $CaCrO_3$ small single crystal and confirmed the AFM transition around the same temperature. The different behavior was also explained, taking into account the effect of grain-boundary scattering in the polycrystalline sample. Also, the possibility of a different stoichiometry was considered as a possible explanation. In 2006, Zhou et al. also reported an insulator-to-metal transition in a polycrystalline sample of this phase under pressure.[22] This confirms an insulating character. On the other hand, the observed bond-length fluctuations suggest a Jahn−Teller (JT) distortion. However, in a very recent study, optical conductivity and reflectivity measurements seem to indicate that "$CaCrO_3$ is metallic, despite being antiferromagnetic" and "that the negative dependence of the resistivity against temperature is due to grain boundary scattering".[40] The PXRD data collected in our samples suggest a room temperature OO phase transition due to the coupling of the JT effect with the orthorhombic distortion.[24] We have confirmed the crystal structures of both $SrCrO_3$ and $CaCrO_3$ by PXRD (Figure 2) and electron diffraction (Figure 3). $SrCrO_3$ has a cubic structure with space group $Pm\bar{3}m$ and a lattice parameter $a = 3.8198(1)$ Å, in good agreement with that previously reported in the literature.[18,21,22]

For $CaCrO_3$, the orthorhombic space group *Pbnm* was confirmed by PXRD, with lattice parameters $a = 5.2911(1)$ Å, $b = 5.3192(1)$ Å, and $c = 7.4893(1)$ Å, in agreement with previous data.[22,39] The main differences between these two structures is clearly understood by looking at the extra reflections $(120)_o$, $(121)_o$, or $(130)_o$ etc., that appear in orthorhombic $CaCrO_3$ as well as by observation of the splitting of many parent reflections. For example the $(211)_c$ reflection in the cubic perovskite splits in $(312)_o$, $(024)_o$, $(132)_o$, and $(204)_o$ in the $CaCrO_3$ pattern, as can be observed in Figure 2, right-side enlargement. The mid-member of the $Sr_{1-x}Ca_xCrO_3$ solid solution, $x = 0.5$, shows an intermediate situation in X-ray diffraction terms. These differences are even more obvious when the electron diffraction and electron microscopy results are analyzed, as follows:

Parts a and b of Figure 3 correspond to the $[001]_p$ and $[100]_p$ zone axis patterns of $SrCrO_3$ and $CaCrO_3$, respectively, where superstructure reflections appear in the last one at $\mathbf{G} \pm (0, k/2, 0)$, $(0, 0, l/2)$, $(0, k/2, l/2)$, where $\mathbf{G}$ represents the reciprocal lattice vector for the parent perovskite reflections. The simultaneous appearance of these three types of superstructure reflections in the $[001]_p$ zone axis (Figure 3b) is due to the formation of twinned domains in the three directions of space, which are better seen in the corresponding electron micrographs; see Figure 4 in ref 24. These

(39) Wheiher, J. F.; Chamberland, B. L.; Gillson, J. L. *J. Solid State Chem.* **1971**, *3*, 529–532.
(40) Komarek A. C. et al. arXiv:0804.1071v1 [cond-mat.str-el].

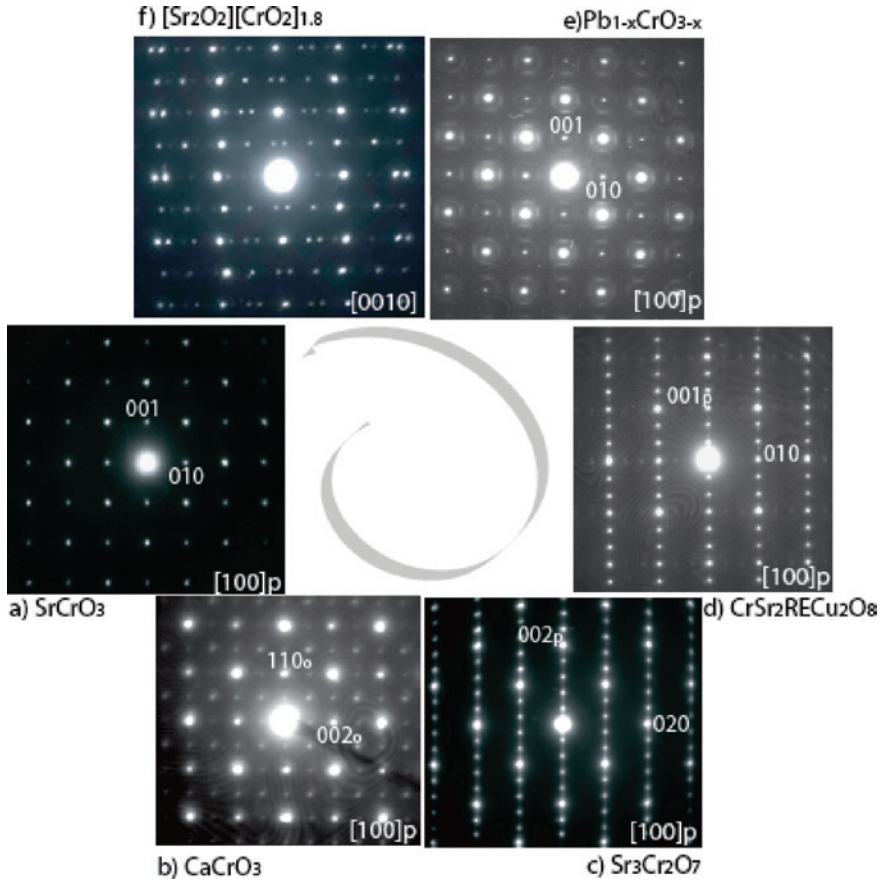

Figure 3. Electron diffraction patterns corresponding to the mixed chromium(IV) oxides, the structures of which are presented in Figure 1 in the same order. The only simple pattern corresponds to cubic $SrCrO_3$ with unit cell a_p and space group $Pm\bar{3}m$ (Figure 3a). All remaining patterns show superstructure diffraction maxima that reflect the increasing structural complexity of these materials. The patterns successively represent the relatively simple superstructure with a diagonal cell $\sim\sqrt{2}a_p \times \sqrt{2}a_p \times 2a_p$, space group *Pbnm*, corresponding to orthorhombic $CaCrO_3$ (Figure 3b), the somewhat more complex perovskite superstructure of tetragonal $Sr_3Cr_2O_7$ ($\sim a_p \times a_p \times 5a_p$, space group *I*4/*mmm*; Figure 3c), and $CrSr_2RECu_2O_8$ ($\sim a_p \times \sim a_p \times 3a_p$, space group *P*4/*mmm*; Figure 3d), the incommensurate modulated superstructure corresponding to $Pb_{1-x}CrO_{3-x}$, and, finally, the pattern corresponding to the misfit-layer structural compound $(Sr_2O_2)(CrO_2)_{1.85}$, unrelated to perovskite and crystallizing in space group $C'nbm(0\sigma 0)00s$ [centering translation vector of ($^1/_2$, $^1/_2$, 0, $^1/_2$)]. Although not obvious in these patterns, the oxides in parts b, d, and e do form 3D microdomains; see the text for full details.

domains are an interesting characteristic of many noncubic perovskites[41−43] and are related to the relative orientation of the long axis of the so-called diagonal cell ($\sim a_p\sqrt{2} \times a_p\sqrt{2} \times 2a_p$) originating in the octahedral tilt along the three space directions. These domains are obviously absent in cubic $SrCrO_3$, where there is no octahedral tilt to induce any supercell.

C. "Solid Solution" $Sr_{1-x}Ca_xO_3$. We have recently prepared, also under high pressure/high temperature conditions and for the first time, the "solid solution" $Sr_{1-x}Ca_xCrO_3$.

We have found that the perovskite structure of $SrCrO_3$ tolerates the increasing distortion produced by the size difference in the A cation site. This changes its structure progressively to an orthorhombic one as the amount of calcium increases together with the octahedral tilt, in common with other solid solutions with the perovskite structure $Sr_{1-x}Ca_xMO_3$ (M = Ti, V, and Fe)[37] as well as in $REMO_3$ (RE = rare earth, M = Ti, V,..., Ni, and Ga).[44] In these examples, as the tolerance factor approaches 1, the structural transformation from orthorhombic to cubic goes through an intermediate tetragonal or rhombohedral structure. This intermediate symmetry is not clearly seen in the $x = 0.5$ composition by checking the splitting of some reflections in the PXRD data (Figure 2); however, electron diffraction shows the appearance of the (h/2, k/2, $^1/_2$) reflections in the cubic perovskite. The system then goes from space group $Pm\bar{3}m$ to space group *I*4/*mcm*, which implies a tilt along one axis [001] to space group *Pbnm*, where the tilt takes place around the three principal axes and can be approximated by a single tilt around $[111]_p$. The appearance of extra reflections in the electron diffraction patterns, as the structure evolves with the substitution of Sr by Ca, is summarized in the schematic representation of two reciprocal cells in Figure 4. The solid black dots are the nodes of the basic perovskite reciprocal sublattice, $x = 0$–0.2. When it becomes tetragonal (space group *I*4/*mcm*), the blue hollow circles appear at $^1/_2(hkl)$ h, k, l = odd ($x = 0.4-0.5$) and they are substituted by the light-blue stars for $x = 0.6$ (see

(41) Alario-Franco, M. A.; Calbet, J. M. G.; Vallet, M.; Grenier, J. C. *J. Solid State Chem.* **1983**, *49*, 219.
(42) Vegas, A.; Vallet-Regi, M.; Gonzalez-Calbet, J. M.; Alario-Franco, M. A. *Acta Crystallogr., Sect. B* **1986**, *42*, 167.
(43) Alario-Franco, M. A.; Henche, M. J. R.; Vallet, M.; Calbet, J. M. G.; Grenier, J. C.; Wattiaux, A.; Hagenmuller, P. *J. Solid State Chem.* **1983**, *46*, 23−40.
(44) Zhou, J. S.; Goodenough, J. B. *Phys. Rev. Lett.* **2005**, *94*, 065501.

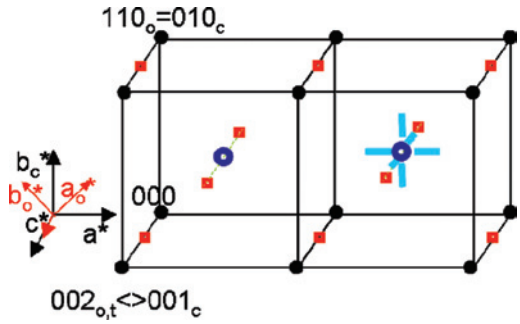

Figure 4. Sketch of two unit cells of the reciprocal lattice or the $Sr_{1-x}Ca_xCrO_3$ solid solution. The different symbols correspond to the following: black solid dots, the cubic subcell ($x = 0-0.2$); hollow dark-blue circles, the extra reflections allowed in the tetragonal cell ($x = 0.4-0.5$); light-blue lines, the extra satellites appearing only for $x = 0.6$. The red squares complete the full reciprocal lattice of the orthorhombic cell ($x = 0.8-1.0$).

below) and complemented with the hollow red squares for the orthorhombic $x = 0.8-1.0$ (space group *Pbnm*).

It is interesting to stress that the idea of a "solid solution", a kind of random distribution between two dissimilar oxides, is certainly somewhat naive because electron microscopy and diffraction show the presence of microdomains in the whole compositional range: that is, as soon as Ca enters the structure, one sees the appearance of satellite reflections and three sets of domains differing in the relative orientation of the diagonal cell of the perovskite superstructure. Even more, there is evidence of JT distortion associated with the tilting in the orthorhombic phases. Interestingly, the domain size seems to be coupled to the composition and domains are bigger closer to the end members than at the middle of the range.[24]

***x* = 0.6 Composition.** From a microstructural point of view, the composition $x = 0.6$ is the most interesting of all of the intermediate phases. Figure 5 shows a series of diffraction patterns obtained after tilting the crystal about the $\langle 100\rangle^*$ and $\langle 110\rangle^*$ reciprocal directions of the cubic perovskite cell. The SAED patterns show some features that are not allowed by the expected space group (*Pbnm*). In the $[0, -1, 1]_p$ zone axis, the reflections consistent with the diagonal cell ($\sqrt{2}a_p \times \sqrt{2}a_p \times 2a_p$) appear at ($h/2$, $k/2$, $^1/_2$). However, in the $[0, -1, 2]_p$ zone axis, sharp satellites appear at $^1/_4$ and $^3/_4$ of $g_{(221)p}$ and $g_{(-221)p}$. These indicate the existence of a supercell of the orthorhombic perovskite with $c = 2a_o = 4a_p$. Also, in the $[1, -1, 3]_p$ zone axis, there are sharp satellites at multiples of $^1/_3$ of $g_{(-332)p}$. They do imply a supercell $c = ^3/_2$, $a_o = 3a_p$. These satellite reflections at ($h/2$, $k/2$, $^1/_2$), ($h/2$, $k/2$, $^1/_3$), and ($h/2$, $k/2$, $^1/_4$) are not discrete reflections but cuts of elongated relrods. The existence of elongated relrods is also suggested by the splitted reflections in the $[0, -1, 3]_p$ zone axes. This is also confirmed by looking at the shape of the satellites in the $[-1, 1, 2]_p$ zone axis or in the splitted reflections along the $[-1, 1, 0]_p$ zone axis appearing at $^1/_2(hkl)$ (enlargement on Figure 5, below the $[0, -1, 1]_p$ zone axis).

When the curvature of the Laue sphere is large enough, the diffraction pattern intersects with four arms directed toward two perpendicular directions. Here the superstructure reflections expected at ($^1/_2$, $^3/_2$ $^1/_2$) (encircled in Figure 5) are splitted into clusters of four spots along $g_{(100)p}$ and $g_{(010)p}$. Therefore, they all can be grouped in a cluster of six rods, the former four plus another two along $g_{(001)p}$ (see Figure 4).

This 6-fold spot splitting could be due to (i) the ordering between Ca and Sr, probably coupled to the microdomains formed by the system of tilted octahedra, as happens in some A-cation-deficient perovskites,[45−47] (ii) the existence of microdomains where the tilting of the octahedra around $\langle 110\rangle_p$ are twinned with domain boundaries along the $\{100\}_p$ directions of the perovskite. It is noteworthy that these crosses do not appear on the basal plane of the reciprocal cell, as happens in, for example, $La_{1/3-x}Li_xNbO_3$ ($^1/_2$, $^1/_2$, 0) reflections[46] but in ($^1/_2$, $^3/_2$, $^1/_2$). This seems to suggest that these satellites are a consequence of the Ca/Sr ordering coupled to the microdomains formed by the system of the octahedral tilt.

Properties. In general, the electronic properties of the different samples of $Sr_{1-x}Ca_xCrO_3$ show a systematic dependence with the composition. All of the samples display low-temperature magnetic singularities. The two end members have the same C-type AFM spin ordering of 1 μB with the spins aligned in the *ab* plane. The magnetic ordering takes place at 50 K for $SrCrO_3$, at 90 K for $CaCrO_3$, and at increasing intermediate temperatures for the rest of the series (Figure 6).

At the temperatures where the magnetic singularities occur, small changes in the slope of the resistance are apparent (Figure 7a). This change in the slope, along with the increased temperature dependence for the Ca-rich samples that happen to have the stronger magnetic interactions, suggests the existence of some coupling between the charge carriers and the magnetic moments. The normalized resistance as a function of the temperature for all samples between 2 and 300 K is shown in Figure 7a. From this plot, one would conclude that all samples are insulators. This agrees with the results that, as indicated above, showed insulator-to-metal transitions under pressure for the end compositions.[22] On the contrary, it has recently been reported that polycrystalline samples that showed a $\rho_{300\ K}/\rho_{2\ K} = 10^{-4}$, typical of an insulator, simultaneously showed a metallic behavior based on optical conductivity data,[25] concluding, then, that grain boundaries are responsible of the high electrical resistance.

It is, nevertheless, intriguing that there is such a dependence with the Ca content of the relative resistivity. In order to put some insight to this problem, we have tested our data on different models for the conductivity of semiconductors;[48] we have found a good correlation with the 3D variable-range-hoping (VRH) conduction mechanism. This is defined by $\rho = \rho_0 \exp[(T_0/T)^{1/(d+1)}]$, where d is the dimensionality of the

(45) García-Martín, S.; García-Alvarado, F.; Robertson, A. D.; West, A. R.; Alario-Franco, M. A. *J. Solid State Chem.* **1997**, *128*, 97.
(46) García-Martín, S.; Alario-Franco, M. A. *J. Solid State Chem.* **1993**, *148*, 93.
(47) Guiton, B. S.; Davies, P. K. *Nature Mater.* **2007**, *6*, 586.
(48) Singleton, J. *Band Theory and Electronic Properties of Solids*; Oxford Master Series in Condensed Matter Physics; Oxford University Press: Oxford, Great Britain, 2003.

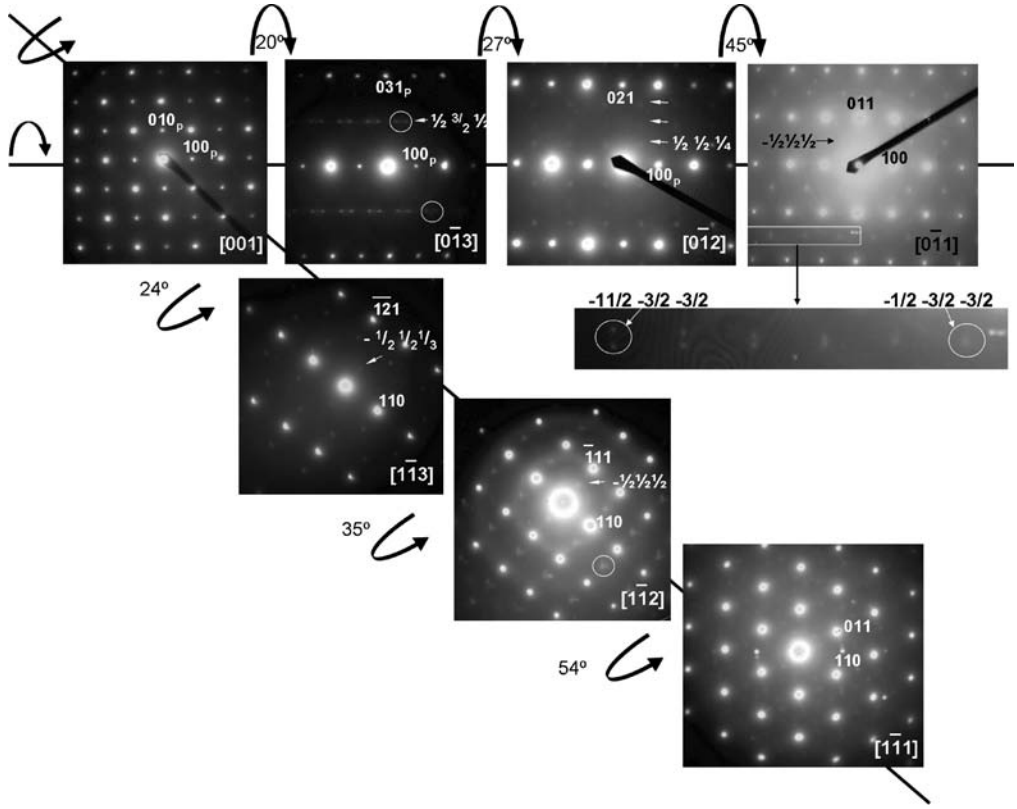

Figure 5. SAED patterns, corresponding to the $x = 0.6$ composition, obtained by tilting along the $\langle 100\rangle_p$* and $\langle 110\rangle_p$* directions. Superlattice reflections form six armed crosses at $^1/_2(hkl)$. Zone axes correspond to the cubic perovskite subcell. Tilt angles were measured from the initial position.

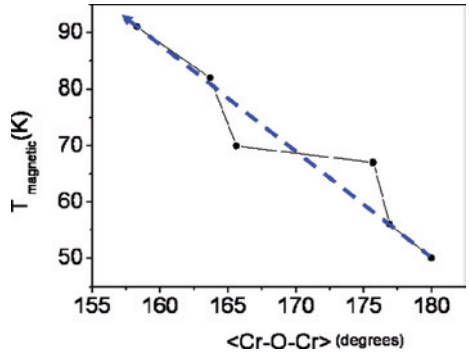

Figure 6. Correspondence between the temperature of magnetic ordering for the different compositions and the average Cr−O−Cr angle determined by PXRD for the $Sr_{1-x}Ca_xCrO_3$ system.

conduction and T_0 is the parameter that relates the resistance and density of states at the Fermi level. Here ln R was plotted against $T^{-1/4}$, and it is found that for all compositions that there is a wide temperature range in which agreement is obtained, and therefore the thermal dependence of our resistance data can be properly described with this model. It is clear that a definite conclusion concerning the transport properties of the different members of the solid solution will be obtained with single-crystal measurements.

D. "Cubic" $PbCrO_3$. Originally $PbCrO_3$ was claimed to have a cubic perovskite structure (space group $Pm\bar{3}m$, $a \approx 4.00$ Å).[20,28] Neutron diffraction studies have shown that this compound has an AFM G-type structure ($a_{mag} = 2a_{nucl}$) at $T_N = 240$ K.[20] Nevertheless, in those works, no clear magnetic signature was observed in the susceptibility measurements.[20,28]

On the other hand, other groups reported an unusual broadening of the diffraction peaks, even using only Cu $K\alpha_1$ radiation.[28] Yet, in these studies, neither was the precise stoichiometry established nor was a microstructural analysis performed.

We have found that, although from PXRD data $PbCrO_3$ appears to be cubic (Figure 2d), the Rietveld refinement results in rather high thermal factors, especially for the Pb atom.[29] This fact, together with the peak broadening, which can be compared in Figure 2 with that of the cubic perovskite $SrCrO_3$, suggested the possibility of the Pb being off-center from the ($^1/_2$, $^1/_2$, $^1/_2$) position. This is, in fact, a common characteristic of Pb^{II} and other so-called inert pair cations and has been previously observed in other perovskites (e.g., Pb_2MgWO_6[49]). When this off-centering was taken into account in the refinement, with the introduction of a displacement vector along the main directions within the cubo-octahedral position (namely, $[100]_p$, $[110]_p$, and $[111]_p$), it was observed (Figure 8) that the R_{Bragg} and R_W factors converged on a minimum value for a similar displacement of ~0.3 Å in all of them. This is interpreted as the Pb^{II} cation being split among the resulting 26 positions [respectively 6 along the cell axes, {100}, 12 along the phase diagonals, {110}, and 8 along the cube diagonals,{111}, around the central A position, which is empty (Figure 8)]. Consequently, in every unit cell, the Pb ion is randomly located in one of

(49) Baldinozzi, G.; Sciau, Ph.; Pinot, M.; Grebille, D. *Acta Crystallogr., Sect. B* **1995**, *51*, 668.

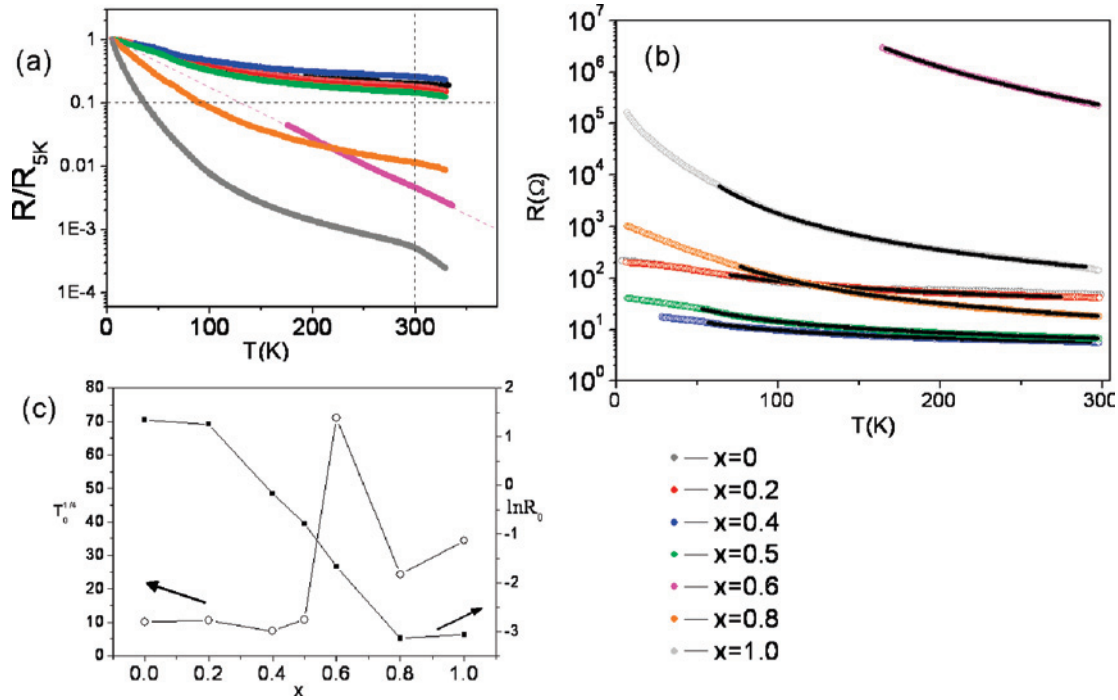

Figure 7. (a) Relative resistance normalized to the resistance at 5 K vs temperatures for the samples $x = 0$, 0.2, 0.4, 0.5, 0.6, 0.8, and 1.0 in $Sr_{1-x}Ca_xCrO_3$. (b) Logarithmic plot of resistance vs temperatures in the range from 300 to 2 K for the same samples. The black solid lines represent the fits to a 3D VRH model. (c) Parameters obtained from the linear fit vs Ca content x.

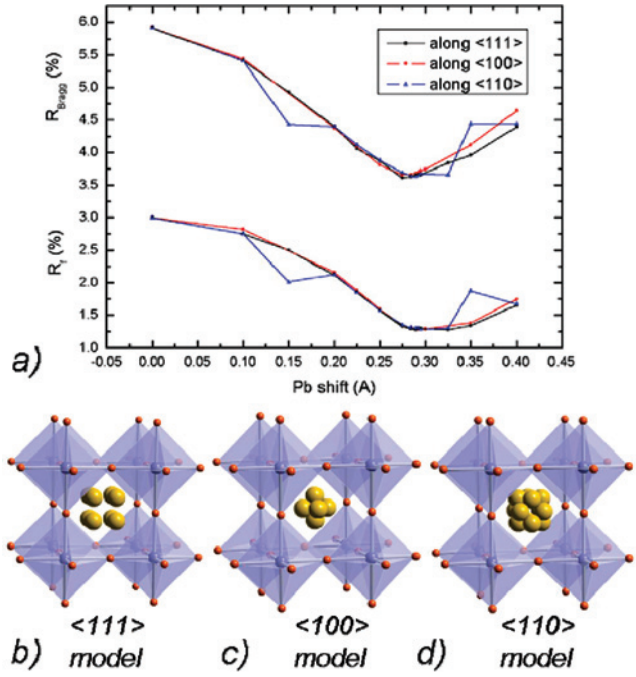

Figure 8. (a) Agreement factors, R_{Bragg} and R_f, in the Rietveld refinement of the PXRD data vs the Pb shift for the average cubic phase of $PbCrO_3$. The three models show the same minimum. An approximate representation of the average structure of $PbCrO_3$ as suggested by X-ray diffraction: Cr sets in a regular oxygen octahedron, while Pb is distributed over a multisplitted A position along the (a) 8-⟨111⟩, (c) 6-⟨100⟩, and (d) 12-⟨110⟩ directions.

those positions; the PXRD pattern averages out the structure of $PbCrO_3$, which then appears as cubic.

Properties. Figure 9a shows the temperature dependence of the susceptibility when cooling from 300 to 2 K measured in ZFC and FC modes at 100 Oe for "$PbCrO_3$". The divergence of the temperature dependence between ZFC and FC magnetization seems to indicate a magnetic transition at 180 K, which would imply some (weak) ferromagnetic interactions. At 30 K, a maximum appears in the ZFC curve, which indicates an AFM transition. The G-type AFM structure observed in this compound at 4.2 K by Roth and DeVries[20] likely corresponds to the transition that we observed at 30 K. Although they located the Néel temperature at 240 K, we did not observe any magnetic anomaly at this temperature, but see below.

The thermal dependence of the electrical resistance shows the semiconducting properties of this phase in the range 210 K $< T <$ 395 K (Figure 9b). Below this temperature, the resistance is too high to be measured with our equipment. The conduction is thermally activated, as can be deduced from the logarithmic plot of the resistance (Arrhenius law $R = R_0 \exp(\Delta E/k_B T$; Figure 9, inset). Interestingly, at 240 K, which is the temperature suggested by Roth and DeVries for T_N, there is a change in the activation energy, from 0.11 eV at high temperature to 0.26 eV at lower temperature. The discrepancy between the early reports and our results might be explained by the complex microstructure present in this phase (see section IV).

As mentioned above, $PbCrO_3$ belongs to the series in which both $PbTiO_3$ and $PbVO_3$ are tetragonal and ferroelectric,[50−52] something that is attributed to the presence of the lone pair in Pb^{II}. However, $PbCrO_3$ was claimed to be cubic and, consequently, not ferroelectric. In view of the random-

(50) Shirane, G.; Susuki, K.; Takeda, A. *J Phys. Soc. Jpn.* **1952**, *7*, 12–19.
(51) Shpanchenko, R. M.; Chernaya, V. V.; Tsirlin, A. A.; Chizhov, P. S.; Sklovsky, D. E.; Antipov, E. V. *Chem. Mater.* **2004**, *16*, 3267–3273.
(52) Kumar, A.; Martin, L. W.; Denev, S.; Kortright, J. B.; Suzuki, Y.; Ramesh, R.; Gopalan, V. *Phys. Rev. B* **2007**, *75*, 060101R.

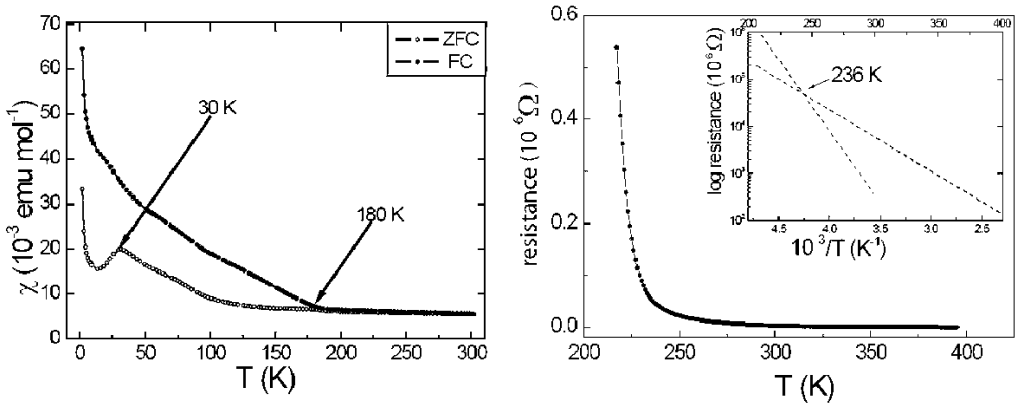

Figure 9. (a) Thermal dependence of the magnetic susceptibility of "$PbCrO_3$" showing two magnetic anomalies at 180 and 30 K, respectively. (b) Resistance vs temperature. Inset: Arrhenius plot with two linear regions. Activation energies are 0.26 and 0.11 eV for the low- and high-temperature ranges, respectively.

ization of the Pb in the 26-splitted A position, it is clear that the inert pairs will also be randomized, resulting in a paraelectric state.

II. RP Phases $Sr_{n+1}Cr_nO_{3n+1}$. The well-known RP phases, $A_{n+1}M_nO_{3n+1}$, one of the types of the so-called *layered* perovskites, are among the best known perovskite derivatives.[53] Their structure is more commonly described as an intergrowth of single rock salt (RS) type AX "layers" and increasingly thick perovskite AMX_3 blocks and can then be formulated as $nAMX_3 + AX$ (e.g., $Sr_3Cr_2O_7$ for $n = 2$ in Figure 1).[17] These RP materials have received a great deal of attention for their metallic, ferromagnetic,[54] colossal magnetoresistance,[55] superconducting,[56] and, more recently, thermoelectric properties.[57]

Interestingly, there is a polymorph for the RP1 member, i.e., $Sr_2Cr^{IV}O_4$,[58,59] synthesized without high pressure; it has the β-K_2SO_4 structure type in which Cr^{IV} is in a tetrahedral environment. The only other mixed strontium−chromium(IV) oxide that can be made at room pressure is $Sr_4Cr_3O_9$. It has two Cr^{III} and one Cr^{IV} in octahedral coordination.[60]

In 1972, the RP phases with $n = 1$ and 2 (Sr_2CrO_4 and $Sr_3Cr_2O_7$) were synthesized at 65 kbar. The space group *I*4/*mmm*[61] was determined by means of PXRD. However, no detailed study of the structure, microstructure, or properties of these compounds was carried out.

RP $n = 1$. In 2007, the RP1, Sr_2CrO_4, was successfully synthesized from a fluoride precursor at ambient pressure,[62] and it has been shown to be a Curie−Weiss paramagnet in which AFM interactions do not originate any long-range order down to 2 K. We have also prepared this compound under high pressure (Table 1). However, the high-pressure-synthesized phase, RP1, is unstable and rapidly oxidizes to $Sr_3Cr_2O_8$ (with the palmierite structure,[63] at room conditions) plus $SrCrO_3$ and $SrCO_3$ [$3Sr_2CrO_4 + {}^1/_2O_2 \rightarrow Sr_3Cr_2O_8 + SrCrO_3 + 2SrO$ ($+2CO_2 \rightarrow 2SrCO_3$)]. This is, indeed, a rare (if not the only) example of a Cr^{IV} to Cr^{V} oxidation at room pressure and temperature!

Interestingly, the high-pressure-synthesized RP1 compound has smaller lattice parameters than the product obtained from the fluorides; it also has a smaller *c*/*a* ratio (3.27 vs 3.31 for the product from fluoride synthesis and 3.24 for the original one obtained in 1972 by Kafalas and Longo).

RP $n = 2$. We have also synthesised at high pressure the RP2 member, which is much more stable at ambient conditions.[26] Rietveld refinement of the PXRD data in the space group *I*4/*mmm* gave the expected structure (Figure 1). However, as happens in the $Sr_3Ti_2O_7$ phase,[64] it also shows an axial distortion in the [Cr−O_6] octahedra, which are compressed toward the perovskite block and elongated toward the RS-type layer. Moreover, the Cr atoms are displaced off-center toward O1 (as indicated by thick arrows in Figure 10). The nine-coordinated Sr atom, however, is displaced toward O3. This results in the SrO layers, and to a smaller extent the [Cr−O_2] layers, being slightly folded in a zig-zag fashion, as indicated by thin arrows in Figure 10. The average ⟨Cr−O⟩ distance is 1.917 Å, for which a radius of 0.56 Å is obtained for Cr; this is in good agreement with the Shannon radius for octahedrally coordinated Cr^{IV},[65] which is given as 0.55 Å.

Electron Microscopy Observations. Figure 11 shows a HRTEM image of RP1 in which the structure can clearly be discerned.

The characteristic feature of RP2 phases is the body centering of the lattice, I, formed by two perovskite blocks separated by a RS layer, which results in a 5-fold

(53) Greenblatt, M. *Curr. Opin. Solid State Mater. Sci.* **1997**, *2*, 174–183.
(54) Battle, P. D.; Burley, J. C.; Cussen, E. J.; Hardy, G. C.; Hayward, M. A.; Noailles, L. D.; Rosseinsky, M. J. *Chem. Commun.* **1999**, *19*, 1977.
(55) Morimoto, Y.; Asamitsu, A.; Kuwahara, H.; Tokura, Y. *Nature* **1996**, *380*, 141.
(56) Bednorz, J. G.; Müller, K. A. *Z. Phys. B Condensed Matter* **1986**, *64*, 189.
(57) Koumoto, K.; Terasaki, I.; Funahashi, R. *MRS Bull.* **2006**, *31*, 206.
(58) Wilhelmi, K. A. *Ark. Kemi* **1966**, *26*, 157.
(59) Chamberland, B. L.; Herrero-Fernandez, M. P.; Hewston, T. A. *J. Solid State Chem.* **1985**, *59*, 111.
(60) Cuno, E.; Müller-Buschbaum, Hk. *Z. Anorg. Allg. Chem.* **1989**, *572*, 175.
(61) Kafalas, J. A.; Longo, J. M. *J. Solid State Chem.* **1972**, *4*, 55–59.
(62) Baikie, T.; Ahmad, Z.; Srinivasan, M.; Maignan, A.; Pramana, S. S.; White, T. J. *J. Solid State Chem.* **2007**, *180*, 1538–1546.
(63) Negas, T.; Roth, R. S. *J. Res. Natl. Bur. Stand. A* **1969**, *73*, 431.
(64) Elcombe, M. M.; Kisi, E. H.; Hawkins, K. D.; White, T. J. *Acta Crystallogr., Sect. B* **1991**, *47*, 305.
(65) Shannon, R. D. *Acta. Crystallogr., Sect. A* **1976**, *32*, 751.

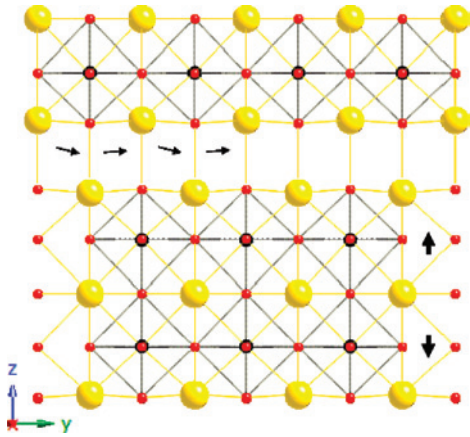

Figure 10. View of the structure of $Sr_3Cr_2O_7$ projected along $[100]_{RP}$. Observed atomic shifts are indicated by arrows; see the text for details.

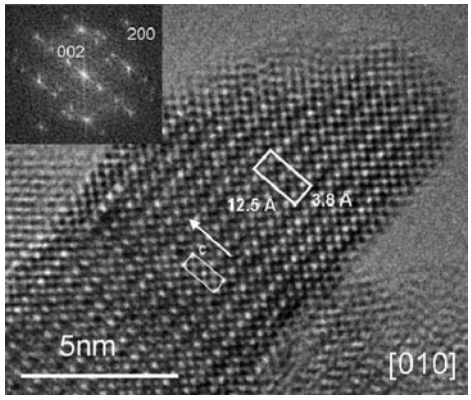

Figure 11. HRTEM image of Sr_2CrO_4 along the zone axis [010]. One of the white rectangles highlights the unit cell, and the other one, the image simulation. The corresponding FFT is shown on the upper left corner.

periodicity along the *c* axis. This is the origin of the five spacings found from 000 to "002_p" (or 0010_{RP}) in the electron diffraction pattern, shown in Figure 3c. As frequently happens in RP phases, intergrowths with higher order members were frequently found in electron microscopy observations; these are responsible for the streaking found along the *c** axis in the same pattern. Moreover, a quite complex microstructural variety was found with both orthorhombic and tetragonal crystals, which very often present extra satellite reflections originating from both commensurate and incommensurate superstructures in the *ab* plane.[26] On the other hand, twinned microdomains typically found in orthorhombic perovskite-based materials cannot be observed in this structural type.

Evidence of two new phases, RP3 ($n = 3$) and a 15R, formed at 80 kbar was also obtained by electron microscopy.[26] The observed $SrCrO_3$-15R phase is the first example of a hexagonal perovskite in the Sr−Cr−O system; these types of phases were already well-known in the Ba−Cr−O system. Like with other transition metals, a hexagonal perovskite is obtained as a result of the large size of Ba ($r_{Ba} = 1.61$ Å).[65] In 1969, Chamberland obtained several phases, 4H, 6H, 9R, 12H, 14H, and 27R,[66] by working at similar high-pressure and high-temperature conditions, with the reaction time being the key factor for the preferential

(66) Chamberland, B. L. *Inorg. Chem.* **1969**, *8*, 286.

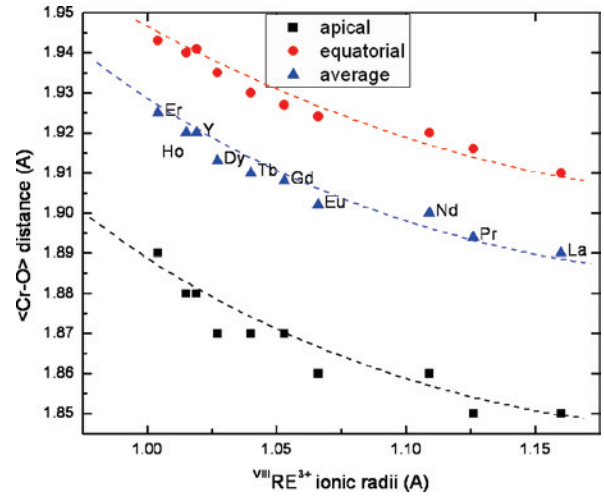

Figure 12. Cr−O distances in the $[Cr-O_6]$ octahedra in the Cr-1212 family vs ionic radii of $^{VIII}RE^{3+}$; the lines are a visual aid.

synthesis of the different phases. An oxygen-deficient five-layer $BaCrO_{2.90}$ phase was also reported to be obtained at ambient pressure in 1975.[67]

Properties. The $n = 2$ member of the RP family presents a broad maximum in the magnetic susceptibility curves analogous to that found in other RP phases such as $Sr_3Rh_2O_7$.[68] The maximum has a cusp around 200 K, which also corresponds to an anomaly observed in the heat capacity data.[26] The thermal functionality of the electrical resistance has a higher slope than that of the cubic perovskite. Both can be described by a VRH mechanism.[48,69]

III. Chromo Cuprates $Cr^{IV}Sr_2RECu_2O_8$. We have recently reported the preparation and characterization of 11 members of the family $CrSr_2RECu_2O_8$ with RE = La, Pr, Nd, Eu, Gd, Tb, Dy, Y, Ho, Er, and Lu.[30] This family was synthesized in the pressure range of 60−80 kbar and at 1300 °C for 30 min. In these types of M-1212-type oxides, there is, in fact, a very interesting gaussian relationship between the optimum synthesis pressure and the rare-earth ion size, which does not follow the well-known "lanthanide contraction". This is discussed elsewhere.[70]

The PXRD patterns of the different members of the family were indexed in a tetragonal cell (space group *P4/mmm*). All of these materials are isomorphous with the Ru analogues $RuSr_2RECu_2O_8$.[71] Nevertheless, although the structure is similar to that observed for the rutheno cuprates, there are some interesting differences with respect to it.

The evolution of $[Cr-O_6]$ octahedral dimensions does follow the lanthanide contraction (Figure 12), and their corresponding unit cell volume decreases upon an increase in the the rare-earth ionic radii. This is a strong indication of the importance of ionic bonding in this structure. The

(67) Torii, Y. *Chem. Lett.* **1975**, *557*, 562.
(68) Yamaura, K.; Huang, Q.; Young, D. P.; Noguchi, Y.; Takayama-Muromachi, E. *Phys. Rev. B* **2002**, *66*, 134431.
(69) Castillo-Martínez, E. Ph.D. Thesis, Universidad Complutense de Madrid, Madrid, Spain, 2008.
(70) Alario-Franco, M. A.; Ruiz-Butos, R.; Dos Santos-García, A. J. *Inorg. Chem.* **2008**, *47*, 6475–6481.
(71) McLaughlin, A.; Zhou, W.; Attfield, J. P.; Fitch, A. N.; Tallon, J. L. *Phys. Rev. B: Solid State* **1999**, *60*, 7512.

[Cr−O_6] octahedra are, in all cases, elongated, i.e., $d_{apical}/d_{equatorial} > 1$, but this ratio is practically constant for any member. From the average ⟨Cr−O⟩ distance in the different members (Figure 12), an ionic radius of ∼0.55 Å is obtained; this is in excellent agreement with that expected for six-coordinated Cr^{IV} in oxides.

On the other hand, copper is five-coordinated in a square pyramid, and there are two different distances: four short equatorial and a long apical one, e.g., $d_e \approx 1.93$ Å and $d_a \approx 2.1$ Å, respectively when RE = Y. Because the equatorial distances of both polyhedra are slightly different, there is a small misfit between the charge reservoir layer and the copper planes, and this is the reason for the polyhedra being tilted away from the *c* axis. Moreover, the apical Cu−O distance in the pyramid is very short, ∼2.10 Å. In fact, this is the shortest apical d_{Cu-O} value ever observed in these types of materials.

Electron Microscopy Observations. HRTEM studies confirmed the average tetragonal crystal structure, but they also showed a more complicated microstructural situation. Instead of the usual triple perovskite superstructure, characteristic of the HTSC cuprate materials, namely, $\sim a_p \times a_p \times 3a_p$, we observed in here the so-called diagonal perovskite superstructure with parameters $\sim a_p\sqrt{2} \times a_p\sqrt{2} \times 3a_p$, which is due to the tilting of the [Cr−O_6] octahedra. Moreover, in all of the studied crystals, a microdomain texture is present as in other perovskite-based compounds; e.g., see the cases of $CaCrO_3$ and of "$Pb_{1-x}CrO_{3-x}$" below as well as refs 41, 42, 74–77 and 94 for a full discussion of this interesting microstructural topic. These domains are intergrowth in three dimensions, so that the triple perovskite-based axis ($c = 3a_p$) alternates, in each domain, along one of the three space directions. The SAED pattern shown in Figure 3d corresponds to a crystal region that presents almost only one domain; however, faint reflections corresponding to the triple cell in a perpendicular direction, corresponding to a minority perpendicular domain, can also be observed.

Properties. In the study of the magnetic susceptibility of these compounds, none of the prepared materials were found to be superconducting. Two types of magnetic behavior were observed, depending upon the magnetic nature of the rare earth in the structure. When RE was Y or La, an AFM transition was observed at ∼130 K (Y) and at ∼150 K (La), corresponding to the ordering of the Cr magnetic moments. However, the materials containing a magnetic rare earth, such as Gd, Dy, and Ho, showed paramagnetic behavior with low susceptibility values[30] down to 4 K.

The short apical Cu−O distance in the [Cu−O_5] pyramid is undoubtedly related to Cu being in an intermediate "2.5+" oxidation state,[72] i.e., 50% Cu^{II} and 50% Cu^{III}. As appears from a plethora of experimental data,[73] for superconductivity to be observed in the HTSC cuprates, the charge on the Cu atoms in the conducting planes has to be included between ∼2.05+ and ∼2.25+. Although still unexplained, this seems to be a crucial factor and, indeed, it is present in all superconducting cuprates.[74]

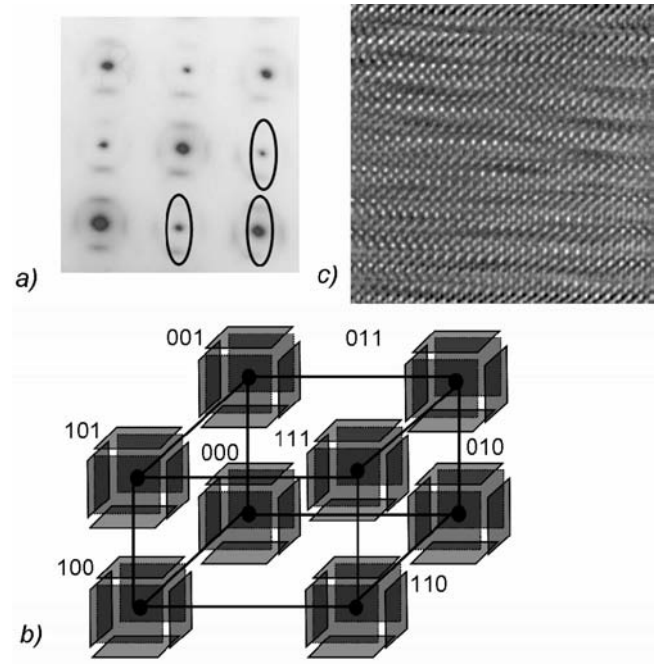

Figure 13. Image reconstruction by using just one set of rods along one of the principal directions in "$PbCrO_3$": (a) Section of the electron diffraction pattern along the [001] ZAP with the diffuse scattering along one direction encircled; (b) corresponding reciprocal lattice; (c) filtered HRTEM image selecting the main spots and the streaks along only one direction.

IV. "$PbCrO_3$" as an Incommensurate Modulated Structure. When studied by electron diffraction and microscopy, $PbCrO_3$ appears far more complex than what PXRD indicates;[29] see paragraph I-D above.

The $[001]_p$ zone axis of $PbCrO_3$ (Figure 13) shows, besides the main perovskite spots, kinds of rods. After detailed tilting experiments, these rods were shown to be due to the presence of planes of diffuse scattering around the main spots and at $^1/_3a_p^*$ from them along the $g_{(100)}$ reciprocal directions. At that point, by means of XEDS in the electron microscope, detailed in situ analysis was done, and it showed a substantial Pb deficiency in the sample. This was estimated to be on the order of 10%, indicating an approximate formula $Pb_{0.9}CrO_{2.9}$. This suggests that the presence of the diffuse scattering is likely to be related to the Pb deficiency. In fact, a very detailed electron diffraction and microstructural study did show the existence of a modulation of the Pb occupation factor in the structure, which is schematically represented on Figure 14. On the other hand, this modulated occupation, in the light of the PXRD data and previous experience in related A-cation-deficient perovskites,[75−77] is likely to be accompanied by a displacement modulation. This modulation of the crystal structure shows itself within three sets of microdomains in which it is oriented at random in the three

(72) Ruiz-Bustos, R. Ph.D. Thesis, Universidad Complutense de Madrid, Madrid, Spain, 2003.
(73) Alario-Franco, M. A. *Yearbook of Science and Technology*; McGraw-Hill: New York, 2008.
(74) Takayama-Muromachi, E. *Chem. Mater.* **1998**, *10*, 2686.
(75) García-Martín, S.; Alario-Franco, M. A.; Ehrenberg, H.; Rodríguez-Carvajal, J.; Amador, U. *J. Am Chem. Soc.* **2004**, *126*, 3587.
(76) Alario-Franco, M. A.; Grey, I. E.; Joubert, J. C.; Vincent, H.; Labeau, M. *Acta. Crystallogr., Sect. A* **1982**, *38*, 177.
(77) Labeau, M.; Grey, I. E.; Joubert, J. C.; Vincent, H.; Alario-Franco, M. A. *Acta Crystallogr., Sect. A* **1982**, *38*, 753.

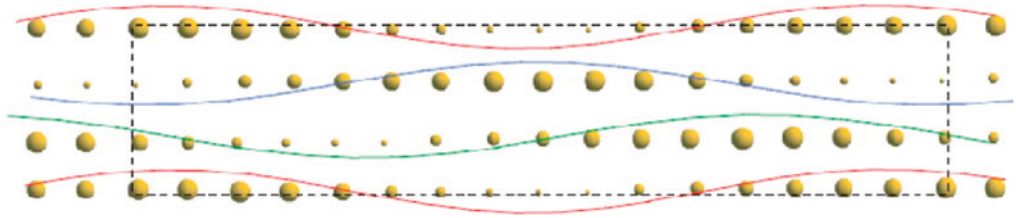

Figure 14. Schematic representation of the occupational modulation of the Pb atoms at the A position of the basic perovskite cell, as represented by their size. The lines are a guide to the eye showing the shape of this modulation. The unit cell in two dimensions ($3a_p \times \sim 16a_p$) is indicated by the dashed line (the third axis is just a_p); see the text for details.

space directions. Image reconstruction by using just one set of the rods along one of the principal directions shows (Figure 13a,b) (i) that the modulation goes, in each domain, along one of those directions and (ii) a dephasing in the modulation of $3a_p$ along a perpendicular direction, which corresponds to the distance at which the diffuse scattering planes are located with respect to the main perovskite spots in the reciprocal lattice (Figure 13c). As expected, when the filtering is performed with the corresponding perpendicular is set, not shown, the modulation appears in the perpendicular direction.[29] Obviously, one cannot make the filtering with the third set of rods (along $g_{(001)}$) because at this orientation they are not intersected by the Ewald sphere. Yet, by the symmetry of the reciprocal lattice, the modulations, and the dephasing, are distributed at random in microdomains in the three space dimensions.[29]

V. Misfit-Layer Structure $[Sr_2O_2][CrO_2]_{1.85}$. We have recently found in the Sr−Cr−O system new phases that adopt a misfit-layer structure (MLS) type. These structures are formed by two different layered type structures, having in common a lattice parameter along one of the layer directions and another different lattice parameter on the other layer direction; the third one indicates the stacking.[78−80]

We have observed that MLS phases in the $Sr-Cr^{IV}-O$ system form in a wide range of pressures and temperatures above 35 kbar and that at higher pressures they can coexist with the perovskite and RP2 phase. However, no intergrowth of these phases in the same crystal is observed.

The PXRD data (Figure 15) show a very rich pattern in which a few very intense peaks correspond to *d* spacings that are all integers of 1.5 Å. They correspond to the 00*l* reflections and indicate a preferential orientation in this layered material. This fixes the value of the *c* parameter. In order to fully determine the structure of this compound, other diffraction techniques are necessary.

A typical electron diffraction pattern of this structure is seen in Figure 3f. It can be seen that there are two sets of intense main reflections, corresponding to the two layered type cells, along with a set of weaker satellite reflections, which are a consequence of the modulation of one layer type with respect to the other and are clear proof of its existence. The electron diffraction study shows that several misfit-layer phases are, in fact, obtained under these conditions.[81] They

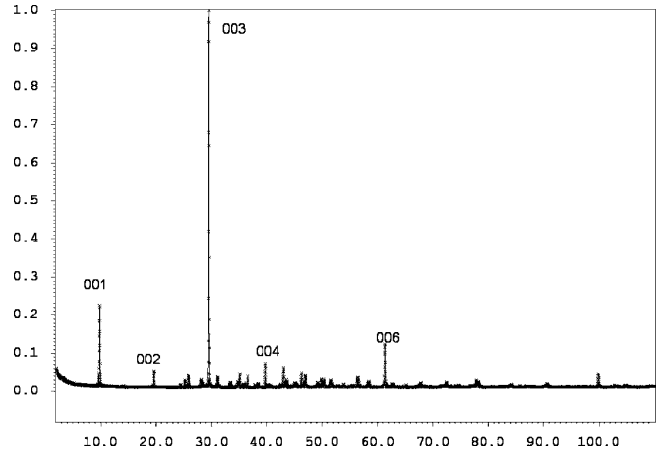

Figure 15. PXRD of the misfit-layer oxide $Sr_2O_2[CrO_2]_{1.85}$. The 001 diffraction maxima, indicating the preferential orientation of the crystals, are indicated.

are all composed of a two-atoms-thick RS layer, SrO, which alternates along the stacking direction with a $[Cr-O_2]_\infty$ layer that can be described as a (001) CdI_2 type. In this layer, Cr is at the center of oxygen octahedra, which contrary to all the above perovskite related materials do not share vertexes but form a flat layer of lying octahedra sharing six edges (Figure 16f). The structure of a twinned orthorhombic polytype is shown in Figure 1. Its incommensurate modulated crystal structure has been solved in a single-crystal diffraction study.[27] The Cr−O distances are slightly modulated as corresponding to a composite crystal, with an average value, in this polytype, of ~2.01 Å, larger than the corresponding sum of Cr^{4+} and O^{2-} ionic radii.

Properties. Magnetic susceptibility measurements also show a 2D character as expected in this structural type because the layers containing magnetic cations are separated 9 Å apart from each other. The electrical resistance in polycrystalline samples is also very high, compared with the perovskite-related phases.

EELS

Because EELS measurements involve the excitation of electrons from a core level to partially filled and empty states, the peak position and spectral line shape in the EEL spectra give information about the oxidation state and coordination of the components. With this in mind, an EELS study comparing the features of the spectra of all of these high-pressure chromium oxides with those of the well-known Cr_2O_3 and CrO_2 has been performed along with that of a chromium(III) perovskite ($BiCrO_3$). It is to

(78) Makovicky, E.; Hyde, B. G. *Struct. Bonding* **1981**, *46*, 101–170.
(79) Otero-Diaz, L. C.; Fitzgerald, J. D.; Williams, T. B.; Hyde, B. G. *Acta Crystallogr., Sect. B* **1985**, *41*, 405.
(80) Van Smaalen, S. *J. Phys. Condensed Matter* **1989**, *1*, 2791.
(81) Castillo-Martínez E. To be published.

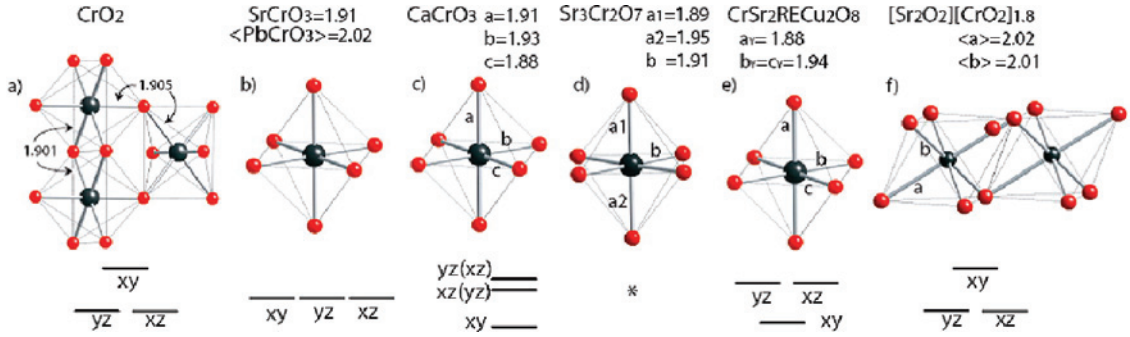

Figure 16. Octahedral [Cr−O_6] distortions observed in the compounds studied in this work. The corresponding qualitative splitting of the t_{2g} energy levels is also shown below each figure. The asterisk corresponds to an intermediate situation between that of CrO_2 and Cr-1212.

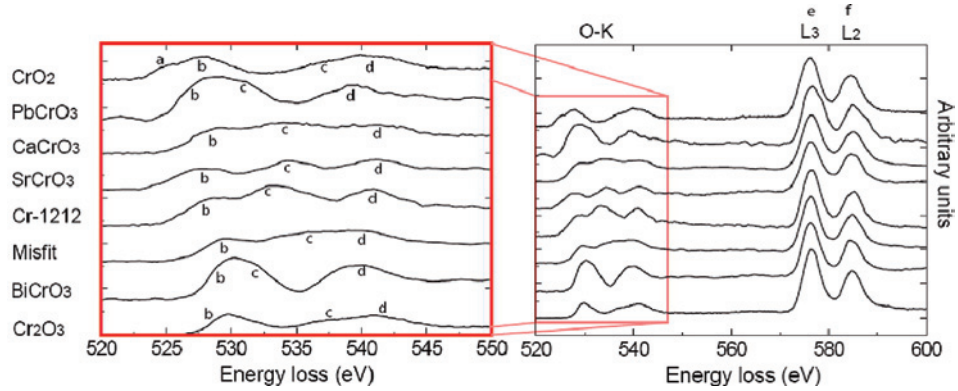

Figure 17. Experimental EELS spectra for the studied Cr compounds. The spectra corresponding to CrO_2, Cr_2O_3, and $BiCrO_3$ are shown as reference values for Cr^{IV} and Cr^{III}.

be pointed out that the oxidation state in chromium compounds cannot be resolved unambiguously with only the Cr $L_{2,3}$ edges: even CrO_2 and Cr_2O_3 do not show many differences in this peak region.[82,83] Nevertheless, Cr L_3 is used to normalize the spectra, and we are able to compare the different features on the O−K edge. Figure 17 displays the EEL spectra for the O−K and Cr $L_{2,3}$ of the following samples: CrO_2, "$PbCrO_3$", $CaCrO_3$, $SrCrO_3$, Cr-1212, $[SrO]_2[CrO_2]_{1.8}$, $BiCrO_3$, and Cr_2O_3. In the O−K region, one can observe notable differences between the various compounds, even among the three chromium(IV) perovskites.

CrO_2 presents a spectrum with four maxima, namely, a−d. The first one, a, was attributed[82] to arise from the introduction of holes into the O 2p orbitals. This was confirmed by LSDA+U calculations, and CrO_2 was described as a self-doped double-exchange ferromagnet.[84] The other three peaks are also present in Cr_2O_3 but at different energies. The b maximum is due to the O 2p states hybridizing with the transition-metal 3d band, while c and d come from hybridization of the O p state with the 4s and 4p states of the chromium.[85]

In the oxides under study, the corresponding three last maxima (b−d) are also present, but the a peak seems to be a unique feature of CrO_2 despite these compounds being in the same oxidation state.

As a general trend in all of the phases studied, one can see that (i) the b peak energies spread between the limits imposed by the b maxima of CrO_2 and Cr_2O_3, (ii) the c peaks are clearly visible, have higher intensity than the ones belonging to the binary oxides, and are dispersed at lower energies, and (iii) the d peak energies are extended over a range of 2.1 eV. Because c and d depend on the A cation, they show the larger differences among the studied compounds.

In the spectrum of "$PbCrO_3$", the c peak is not well-resolved; it is shifted to lower energies (529.1 eV), coalescing with the broad b peak. This peak is attributed to the O p state hybridized with the Pb p states. This spectrum is similar to that of $BiCrO_3$, where Bi also has a lone pair. However, the b peak of the O−K edge in $BiCrO_3$ appears at higher energies than those of $PbCrO_3$ and is comparable to those of Cr_2O_3 (Table 2).

The perovskites $CaCrO_3$ and $SrCrO_3$ and the Cr-1212 family present similar spectra. This is not surprising because calcium and strontium are alkaline earths and the Cr-1212 phases have a $SrCrO_3$ block. The peak c arises not only from interactions of the oxygen with the 4s states of the chromium, as in CrO_2 or Cr_2O_3, but also from interactions with the other cations via O p−M d hybridization. This is why in Cr-1212, where there are Cu−O and RE−O interactions, the c maximum is located at lower energies.

In the case of the misfit-layered compound $[SrO]_2$-$[CrO_2]_{1.85}$, the main feature of the spectrum resembles that of Cr_2O_3, but it is displaced to lower energies. Besides, the peak c is more pronounced in this case because of the O−Sr interaction but is displaced to higher energies, compared with

(82) Suzuki, S.; Tomita, M. *Jpn. J. Appl. Phys.* **1997,** 36, 4341.
(83) Daulton, T. L.; Little, B. J. *Ultramicroscopy* **2006**, *106*, 561–573.
(84) Korotin, M. A.; Anisimov, V. I.; Khomskii, D. I.; Sawatzky, G. A. *Phys. Rev. Lett.* **1998**, *80*, 4305–4308.
(85) De Groot, F. M. F.; Grioni, M.; Fuggle, J. C.; Ghijsen, J.; Sawatzky, G. A.; Petersen, H. *Phys. Rev. B* **1989**, *40*, 5715.

Table 2. Energy Positions of the O−K and Cr $L_{2,3}$ Edges in the EELS Spectra Shown in Figure 11[a]

compound	peak a ± 0.5 (eV)	peak b ± 0.5 (eV)	ΔE_{cb} (eV)	peak c ± 0.5 (eV)	ΔE_{dc} (eV)	peak d ± 0.5 (eV)	peak e ± 0.5 (eV)	ΔE_{fe} (eV)	peak f ± 0.5 (eV)	⟨Cr−O⟩ (Å)
CrO_2	525.3	527.7	9.4	537.1	3.2	540.3	576.3	8.2	584.5	1.90
"$PbCrO_3$"		529.1	2.7	531.8	7.7	539.5	576.3	8.6	584.9	2.02
$CaCrO_3$		529.2	5.4	534.6	6.6	541.2	576.3	8.7	585	1.91
$SrCrO_3$		528.1	6.6	534.7	6.4	541.1	576.3	8.4	584.7	1.91
$CrSr_2GdCu_2O_8$		529.1	4.2	533.3	7.2	540.5	576.3	8.6	584.9	1.91
$[SrO]_2[CrO_2]_{1.8}$		529.5	6.6	536.1	3	539.1	576.3	8.4	584.7	2.01
$BiCrO_3$		529.7	1.8	531.5	8.4	539.9	576.3	7.6	583.9	2.00
Cr_2O_3		529.7	7.7	537.4	3.7	541.1	576.3	8.4	584.7	1.99

[a] a−f represent the peak positions in that figure. Δ_{ij} represent the difference between adjacent peaks ($E_j - E_i$). The last column contains the average ⟨Cr−O⟩ distances obtained by Rietveld refinement of the powder X-ray data.

the one of $SrCrO_3$, because of different structural features and the more covalent Sr−O bonds. In this compound, single-crystal X-ray diffraction has established[27] a chromium valence between 3+ and 4+, which agrees with the L_3/L_2 intensity ratio criteria.

From the EEL spectra, one can conclude that $CaCrO_3$, $SrCrO_3$, and Cr-1212 are clearly chromium(IV) oxides and indicate a possible mixed-valence oxidation state for the modulated structures.

Discussion

Figure 1 shows the increasingly complex structures that are obtained by high-pressure synthesis starting from CrO_2, while their electron diffraction patterns appear in Figure 3. Both of them are clear proof of the increasing complexity of the different oxides studied. The formation of microdomains is observed in some of these materials. This is the case of "$PbCrO_3$", $CaCrO_3$, and the solid solution $Sr_{1-x}Ca_xCrO_3$ but also of the cation-ordered Cr-1212-RE materials. This is a common phenomenon in distorted perovskites, where the degree of octahedral tilt is not too large and allows the interchange of axes. However, the intrinsic characteristics of the lattice, an alternate stacking between the RS- and perovskite-type layers in RP2 and another one between the RS- and CdI_2-type in the misfit layer, prevent the formation of microdomains. Indeed, we have not found them in the layered derivative RP phases nor in the misfit-layer compounds.

[$Cr^{IV}O_6$] Octahedra. It is interesting to compare the coordination polyhedra about the Cr atom as well as the average interatomic ⟨Cr−O⟩ distances in the different phases. All of these phases have in common the fact that [Cr^{IV}–O_6] octahedra are present in their structure; these are stabilized by the high-pressure synthesis and subsequent quenching. The average ⟨Cr−O⟩ values as obtained from Rietveld refinement of the PXRD data for each compound are listed in the last column of Table 2. The shortest ⟨Cr−O⟩ distance is that found in CrO_2, followed by those of Cr-1212, $CaCrO_3$, and $SrCrO_3$ and far away Cr_2O_3, $[SrO]_2[CrO_2]_{1.85}$, and "$PbCrO_3$". The distances found in the perovskite-type phases, Cr-1212, $Sr_3Cr_2O_7$, $CaCrO_3$, and $SrCrO_3$, where [Cr−O_6] octahedra share the six vertexes, are very close to the distance for Cr^{4+} in CrO_2 (∼1.90 Å), where [Cr−O_6] octahedra share two edges. However, all of these phases present a different type of octahedral distortion (Figure 16).

In the Cr-1212 phases, the ⟨Cr−O⟩ distance ranges from 1.85 to 1.95 Å, all around the 1.90 Å expected for Cr^{4+}. It is interesting to note that the ⟨Cr−O⟩ distance does not increase for the larger RE^{3+} ionic radii, smaller *Z*, as lattice parameters and the cell volume do, but on the contrary, it decreases (Figure 12). This is due to the larger effective charge that f electrons do feel as *Z* increases, which is also responsible for the well-known lanthanide contraction. The less shielded RE cations attract more efficiently the O atoms of the [Cu−O_2] planes. This attraction is transmitted from both ends of the triple perovskite block to the rest of the common structure and results in larger ⟨Cr−O⟩ distances in the central [Cr−O_6] octahedra.

However, in the more complex structures, the two structurally modulated compounds, the ⟨Cr−O⟩ distances are much larger than those corresponding to Cr^{4+} and even bigger than the distances in the [$Cr^{III}O_6$] octahedra of Cr_2O_3 (∼1.99 Å)! For instance, it is ≈2.02 Å for "$PbCrO_3$" and ≈2.01 Å in $[SrO]_2[CrO_2]_{1.85}$. The corresponding larger ⟨Cr−O⟩ distance in "cubic" $PbCrO_3$ with respect to $SrCrO_3$, despite both cations having very similar ionic size and charge (1.49 and 1.44 Å for Pb^{II} and Sr^{II}, respectively[65]), may be related to the influence of the $6s^2$ lone pair of the Pb that with other transition-metal oxides form rather distorted tetragonal perovskites (e.g., $PbTiO_3$[50] and $PbVO_3$[51]). In "$PbCrO_3$", however, it is responsible for the modulated structure, where the Pb atom is in a split position. Both the incommensurability and lead and oxygen understoichiometry could explain the large average bonding distance found in complex $Pb_{1-x}CrO_{3-x}$.

In the case of $[SrO]_2[CrO_2]_{1.85}$, this particular kind of structure seems to be responsible for the long ⟨Cr−O⟩ distance. Besides, the possibility of oxygen nonstoichiometry cannot be ruled out. This is frequently found in misfit-layer cobalt compounds[86] and would imply a valence lower than 4+. Nevertheless, in the case of $SrCr_2O_4$ ($^{IV}Cr^{3+}$),[87] which present the same type of [Cr−O_2] layers, the ⟨Cr−O⟩ distance is 2.045 Å, larger than the expected value for Cr^{3+}, avoiding too short ⟨O−O⟩ distances in this layer type.

The different distortions that the octahedra adopt are represented in Figure 16, where they are indicated by the individual ⟨Cr−O⟩ distances. Below each octahedron, the

(86) Morita, Y.; Poulsen, J.; Sakai, K.; Motohashi, T.; Fujii, T.; Terasaki, I.; Yamauchi, H.; Karppinen, M. *J. Solid State Chem.* **2004**, *177*, 3149–3155.

(87) Pausch, H.; Müller-Buschbaum, Hk. *Z. Anorg. Allg. Chem.* **1974**, *405*, 1.

corresponding splitting of the t_{2g} energy levels that accompany these distortions is sketched for all of the studied compounds except for the asymmetrically distorted octahedron of $Sr_3Cr_2O_7$ because the hybridization expected here prevents us from directly comparing the t_{2g} orbitals. This will, nevertheless, be an intermediate situation between that of elongated octahedra in CrO_2 and that of compressed octahedra in Cr-1212.

In CrO_2 itself, the octahedra are elongated with two long apical distances and four short equatorial ones (Figure 16).[13] The regular octahedron in $SrCrO_3$ and the average one of $PbCrO_3$ have the three t_{2g} orbitals degenerated. Despite the reduction of symmetry to tetragonal *I*4/*mcm*, the [Cr−O_6] octahedra remain almost undistorted up to $x = 0.6$ in the solid solution. For calcium contents equal and/or higher than this composition, the [Cr−O_6] octahedra present a distortion in the basal plane due to the superposition of a cooperative JT distortion to the octahedral tilt. This gives three different pairs of Cr−O distances, as shown on Figure 16c for $CaCrO_3$, and produces a pattern of a long and a short distance in the *ab* plane due to the alternate filling of the d_{xz} or d_{yz} orbitals. The c/a $\approx \sqrt{2}$ ratio means that this is not a static but a dynamic orbital order.[88] The JT effect is not expected to be very strong in a d^2 system, but it seems that the coupling with the octahedral tilt enhances this effect, so that it can be observed at room temperature.[89] In other d^2 perovskites, such as some members of the $REVO_3$ family[90] and the low-temperature phase of $SrCrO_3$,[23] orbital ordering takes place at lower temperatures and determines the resulting AFM spin ordering that takes place at even lower temperatures.

In the RP2 phase, $Sr_3Cr_2O_7$, the ⟨Cr−O2⟩ distance (O2 is at the RS layer) is larger than the Cr−O1 one (O1 is the apical oxygen in the middle of the perovskite block), whereas the four equatorial Cr−O3 distances are equal and intermediate (Figure 16). These long-out/short-in axial M−O distances are also found in $Sr_3M_2O_7$ compounds with M = Ti,[64] V,[91] Zr, Sn,[92] and Ru, but they are opposite when M = Mn,[93] Fe, Rh, or Ir. This phenomenon has not been much explored, and its origin is uncertain.

The Cr octahedra are somewhat flattened in the Cr-1212 series, with two short apical distances d_a and four long equatorial distance d_e (Figure 16). For instance, $d_{ax} \sim 1.88$ Å and $d_{eq} \sim 1.94$ Å when RE = Y.[94] The octahedra are slightly compressed as in the low-temperature tetragonal modification of $SrCrO_3$,[23] ($d_{ax} \sim 1.90$ Å and $d_{eq} \sim 1.91$ Å), but in the Cr-1212 phases, this compression is enhanced by the strong JT effect of the neighboring [Cu−O_5] pyramids. However, the compression is not entirely due to the JT effect of [Cu−O_5] but also to the JT effect of Cr^{4+} because while the [Cr−O_6] octahedra are flattened, [Ru−O_6] octahedra are regular in $RuSr_2GdCu_2O_8$.[95]

Finally, in the misfit-layer oxide $[SrO]_2[CrO_2]_{1.85}$, the Cr−O distances are modulated, and Cr−O_{eq} and Cr−O_{ax} alternate between shorter and longer (see Figure 5 in ref 27). However, the average [Cr−O_6] octahedron is elongated and the average distortion is similar to that of CrO_2. Interestingly, both of these oxides present octahedra that are connected through sharing edges.

Conclusions

The currently known six-coordinated chromium(IV) oxides are reviewed. The use of high pressure and high temperature has allowed us to considerably enlarge the crystal chemistry of Cr^{4+} in binary, ternary, and quaternary oxides. The synthesis conditions specific for each oxide comprise especially narrow windows in pressure and temperature for the RP phases and Cr-1212. Pressures of at least 80 kbar are required for "$PbCrO_3$", while rather low synthesis temperatures are needed for obtaining the $CaCrO_3$ perovksite; also, using CrO_2, nonoxidizing conditions for any Sr−Cr-based oxides other than $SrCrO_3$ are required.

Apart from the classical structures (the cubic $SrCrO_3$ perovskite, the orthorhombic $CaCrO_3$, and the tetragonal RP2 phase), we have recently discovered different complex structural types, already known for other transition-metal oxides, which can also form with Cr^{4+} with the help of high pressure and high temperature. They range from the M-1212-structure type of high-T_c superconductors to the misfit-layer structure type of promising novel thermoelectric oxides. Moreover, a unique microstructure has, for the first time, been observed in the previously called "cubic $PbCrO_3$" corresponding to a compositional modulation of the lead occupation intergrown in three sets of microdomains with a supercell of $a_p \times 3a_p \times 14-18a_p$.

From the electronic point of view, it is interesting to point out that, despite the fact that the parent binary CrO_2 is a half-metallic ferromagnet, other chromium(IV) oxides show AFM interactions, either 2D, as in the RP2 phase and misfit-layer compound as expected for this layered materials, or 3D, as in the perovskites. The Cr-1212 phases show either AFM or paramagnetic behavior, depending on the rare earth. Accompanying this magnetic behavior, a VRH electronic conduction is exhibited by the $Sr_{1-x}Ca_xCrO_3$ solid solution, whereas two Arrhenius laws are followed by the "$PbCrO_3$" perovskite; the RP2 and ML, for their part, show a highly resistive behavior.

This paper has brought out the interest of the crystal chemistry of Cr^{4+} and the richness of their electronic properties. A final point worth noting is the parallelism existing between the chronology of the synthesis and structural complexity. The presence of $PbCrO_3$ in three

(88) Goodenough, B. L. *Struct. Bonding* **2001**, *98*, 1–15.
(89) Lufaso, M. W.; Woodward, P. M. *Acta Crystallogr., Sect. B* **2004**, *60*, 10–20.
(90) Martinez-Lope, M. J.; Alonso, J. A.; Retuerto, M.; Fernandez-Díaz, M. T. *Inorg. Chem.* **2008**, *47*, 2634–2640.
(91) Hintermaier, F.; Helding, S.; Volodarsky, L. B.; Sünkel, K.; Polborn, K.; Beck, W. *Z. Naturforsch.* **1991**, *46b*, 1315–1318.
(92) Green, M. A.; Prassides, K.; Day, P.; Neumann, D. A. *Int. J. Inorg. Mater.* **2000**, *2*, 35–41.
(93) Mitchell, J. F.; Millburn, J. E.; Medarde, M.; Short, S.; Jorgensen, J. D.; Fernández-Díaz, M. T. *J. Solid State Chem.* **1998**, *141*, 599–603.
(94) Ruiz-Bustos, R.; Aguirre, M. H.; Alario-Franco, M. A. *Mater. Res. Soc. Symp. Proc.* **2003**, *755*, DD1.2.1.
(95) McLaughlin, A. C.; Zhou, W.; Attfield, J. P.; Fitch, A. N.; Tallon, J. L. *Phys. Rev. B* **1999**, *60*, 7512.

different regions of this summarizing illustration is particularly noteworthy because, besides their chronological appearance, these three different structures of the same chemical species do indeed represent their increasing complexity. However, this also goes in parallel with the experimental techniques used for their study: PXRD and neutron diffraction in the late 1960s that suggested a simple cubic ABO_3 structure, i.e., the perovskite aristotype; analysis of the agreement factors as a function of atomic displacements from the PXRD data was done 40 years later and gave evidence of a 26-order splitting of the Pb atom in the A position (most likely accompanied by some displacements of the Cr cation in the B position because they did also have somewhat high temperature factors) and finally (up to now), in mid-2007, high-resolution electron microscopy and electron diffraction together with image reconstruction from different parts of the reciprocal lattice and Fourier transform from reciprocal to real space did show the existence of a commensurate modulated superstructure. This is reflecting some lead understoichiometry and indicates a rather big unit cell multiple of the perovskite one ($\sim a_p \times 3a_p \times 16a_p$), which, even more, happens to be distributed at random in the three space directions in the form of microdomains.[29]

We can then end up by quoting the late David Wadsley, who in the late 1970s warned us of the complexities of real solids, indicating that "the structure of a material depends on the wavelength of the observing instrument!".

Acknowledgment. The authors want to thank Dr. Myriam Haydee Aguirre, Dr. Alejandro Durán, Dr. Andreas Schoënleber, and Professor Sander van Smaalen, who contributed to the original works. This work was funded by CICYT (Project MAT2007-64007), Comunidad Autonoma de Madrid (Program MATERYENER, PRICYT S-0505/PPQ-0093, 2006), and Fundación Areces (Ayudas 2004): "Fisica de bajas temperaturas". E.C.-M. and A.M.A.-L. respectively acknowledge UCM and CONACYT for a Ph.D. grant. We also thank the "Luis Bru" Electron Microscopy Center. E.C.-M. and A.M.A.-L. did the work on all oxides but the Cr-1212 family, which was prepared and studied by R.R.-B. M.A.A.-F. designed the overall project and wrote the manuscript, essentially with E.C.-M. and A.M.A.-L.

IC801015B